
# Impact of steel-to-timber joints with screws on the failure modes and reliability of a structurally indeterminate timber beam

Engineering Structures 349 (2026) 121883

Contents lists available at ScienceDirect

Engineering Structures

journal homepage: www.elsevier.com/locate/engstruct

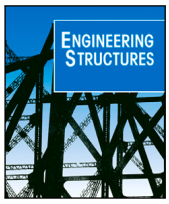

# Impact of steel-to-timber joints with screws on the failure modes and reliability of a structurally indeterminate timber beam

Dorotea Caprio [a,*], Robert Jockwer [b]

[a] Division of Structural Engineering, Department of Architecture and Civil Engineering (ACE), Chalmers University of Technology, Sven Hultins gata 6, 412 96 Gothenburg, Sweden
[b] Chair of Timber Engineering, TUD Dresden University of Technology, George-Bähr-Str.1, 01069 Dresden, Germany

ARTICLE INFO

*Keywords:*
Timber
Reliability
Indeterminate
Nonlinear
Eurocode5
Joints

ABSTRACT

The nonlinear behaviour of timber joints is considered in Eurocode 5 by prescribing a stiffness reduction ratio; specifically, the joint stiffness at the ultimate limit state is calculated as two-thirds of its serviceability limit state value. The system effects, i.e. how the joints interact within the global structure, are not taken into account. These simplifications may be unreliable for modern statically indeterminate structures, potentially leading to non-conservative or overly conservative designs. Steel-to-timber joints with self-tapping screws are widely used and offer high stiffness and load-carrying capacity. This study aims to assess the effects of the current design rules on the reliability of a statically indeterminate timber beam with steel-to-timber joints with self-tapping screws and subjected to a uniformly distributed load. The uncertainties in material properties, the load, and the nonlinear behaviour of joints are considered in the probabilistic model of the structure. For semi-rigid joints with laterally loaded screws, applying the code stiffness reduction ratio of 2/3 roughly doubles the probability of failure compared to the design target. Moreover, the required stiffness reduction ratio is found to be a function of relative joint-beam stiffness and the load-to-screw axis angle. The reliability-based calibrated stiffness ratio ensures that the target probability of failure is met. The framework can also be extended to other joint typologies for safer design.

## 1. Introduction

### 1.1. Background

For many decades, statically determinate systems were the preferred choice in timber construction because of their analytical simplicity. Three-hinged arches were used instead of structurally more efficient two-hinged or clamped end systems, and Gerber systems were preferred instead of continuous purlins [1]. However, as a result of the current building trend to build more complex and structurally challenging structures, engineers increasingly favoured indeterminate systems for their structural efficiency, material economy, and redundancy [2]. This evolution in structural systems has not been matched by a corresponding advance in the level of detail of design approaches. Two shortcomings are identified:

1. Joints are still being idealised as perfectly pinned or clamped with typically linear elastic behaviour [3], even if in reality they are semi-rigid the load–displacement curve is highly nonlinear. Eurocode 5 (EC5) considers the nonlinear load–displacement curve by adopting a stiffness at the ultimate limit state (ULS) $K_{ULS}$ equal to two-thirds of the stiffness at the serviceability limit state (SLS) $K_{SLS}$ [4]. This rule, however, is based on nailed joint tests from the 1960s [5,6] and may be inadequate for other typologies of joints. In fact, laterally loaded nail joints typically show load–displacement curves with low initial stiffness and pronounced ductility, due to the formation of plastic hinges in the fastener. Modern timber joints, for example, those with self-tapping screws that are both laterally and axially loaded in tension, exhibit significantly higher initial stiffness and other failure mechanisms (e.g., head tear-off, withdrawal). Furthermore, the current design approach does not consider the inherent variability in the stiffness and deformation capacity.
2. According to current design approach, design and checks of members are done element by element, typically neglecting system effects on the reliability. However, structures and joints are systems made of interconnected elements.

Ignoring joint nonlinearities and relying on element-by-element design as in EC5 can lead to both over- and under-design of structures at ULS [7]. A system-level analysis is needed, accounting for all member and joint interactions, nonlinear joint behaviour, and variability [8].

* Corresponding author.
*E-mail addresses:* dorotea.caprio@chalmers.se (D. Caprio), robert.jockwer@tu-dresden.de (R. Jockwer).

https://doi.org/10.1016/j.engstruct.2025.121883
Received 5 August 2025; Received in revised form 16 October 2025; Accepted 28 November 2025
Available online 30 November 2025

## Nomenclature

### Abbreviations

| | |
|---|---|
| COV | Coefficient of variance |
| EC0 | Eurocode 0 |
| EC3 | Eurocode 3 |
| EC5 | Eurocode 5 |
| FEM | Finite element model |
| GL | Glulam |
| JCSS | Joint Committee on Structural Safety |
| LVDTs | Linear variable displacement transformers |
| MC | Moisture content |
| MCS | Monte carlo simulation |
| SLS | Serviceability limit state |
| ULS | Ultimate limit state |

### Greek letter

| | |
|---|---|
| $\mathcal{A}$ | Set of active screws |
| $\alpha$ | Moment allocation coefficient (joints) |
| $\alpha_d$ | Design value of rigidity |
| $\beta$ | Moment allocation coefficient (midspan) |
| $\Delta_v$ | Displacement in multi-screw joint |
| $\Delta_{v,inc}$ | Displacement increment |
| $\gamma$ | Load-to-screw axis angle |
| $\rho$ | Person coefficient |
| $\rho_{den}$ | Input variable timber density |
| $\theta_{req}$ | Required rotation at joint |
| $\theta_{max}$ | Rotation at the ends in simply supported beam |
| $\theta_u$ | Ultimate rotation of joints |

### Roman letter

| | |
|---|---|
| $K_{SLS}$ | Stiffness at serviceability limit state |
| $l$ | Beam span |
| $D_f$ | Failure domain |
| $D_{ab}$ | Mean absolute value of ductility |
| $E(\mathbf{X})$ | Demand vector |
| $E_{m,beam}$ | Mean elastic modulus timber |
| $F_{Rd,joints}$ | Lateral resistance of joint |
| $G_k$ | Characteristic value of permanent loads |
| $I_{beam}$ | Beam moment of inertia |
| $K_{10-40}$ | Mean elastic secant stiffness |
| $K_{in}$, $K_p$, $F_t$, $a_1$ | Richard-Abbott model parameters |
| $K_{\theta,d,ULS,joints}$ | Joint required rotational stiffness |
| $K_{\theta,joints}$ | Joint rotational stiffness |
| $K_{ULS}$ | Stiffness at ultimate limit state |
| $M_{Ed,joints}$ | Design bending moment at joint |
| $M_{Ed,field}$ | Design bending moment at midspan |
| $M_{d,max}$ | Design moment at midspan in a simply supported beam |
| $M_{Rd,beam}$ | Bending capacity of the beam |
| $M_{Rd,joints}$ | Bending capacity of the joint |
| $P_f$ | Probability of failure |
| $P_{mod}$ | Vector of model parameters |
| $Q_k$ | Characteristic value of variable loads |
| $R(\mathbf{X})$ | Capacity vector |
| $\mathbf{X}$ | Vector of random variable |
| $Y$ | Vector of material parameters |
| $f_m$ | Input vector of bending resistance |
| $K_{\theta,ULS,joints}$ | Rotational stiffness of the joint |
| $f_{m,d}$ | Design value of the bending resistance |
| $F_{max}$ | Mean load-carrying capacity |
| $F_{multi}$ | Force in the multi-screw model |
| $F_{single}$ | Force in the single-screw model |
| $g(\mathbf{X})$ | Performance function |
| $b_{beam}$ | Beam width |
| $n_{screws}$ | Number of screws |
| $P_{HTO}$ | Probability head-tear off failure |
| $q_{tot,d}$ | Design total (uniform) load |
| $s$ | Couple arm |
| $W_{el}$ | Elastic section modulus of beam section |
| $b_{beam}$ | Beam width |
| $b_{plate}$ | Steel plate width |
| $d$ | Screw diameter |
| $d_{core}$ | Screw core diameter |
| $h_{beam}$ | Beam height |
| $l_{eff}$ | Effective screw length |
| $k_b$ | Joint-beam relative stiffness |
| $k_{mod}$ | Load duration factor |
| $l_{plate}$ | Steel plate length |
| $n_{HTO}$ | Head tear-off cases |
| $n_{tot}$ | Total number of tests |
| $n_{WITH}$ | Withdrawal cases |
| $P_{WITH}$ | Probability withdrawal failure |
| $t_{plate}$ | Steel plate thickness |
| $v_{in,shift}$ | Initial slip |
| $v_u$ | Ultimate displacement |
| $v_y$ | Yielding displacement |
| $z$ | Level arm |

Steel-to-timber joints with self-tapping screws are widely used in various applications due to their strength and stiffness [9,10], particularly in indeterminate structures where load redistribution is crucial. Yet, the reliability of these structures remains unstudied. The next Section reviews joint modelling (Section 1.2) and the impact of joints on structural reliability (Section 1.3), outlining the scope and contributions of this work.

### 1.2. State of the art: models for multi-fastener joints

EC5 design rules derive from the single-fastener behaviour. To extend them to multi-fastener joints, an 'effective number of fasteners' is introduced and exclusively applied to the load-carrying capacity. Stiffness at the serviceability limit state, by contrast, is obtained simply by summing the individual stiffness of all fasteners. The concept of the effective number of fasteners is derived based on several studies that investigated the uneven load distribution of load among fasteners [11–14].

One of the first theories to describe multi-fastener joint behaviour was developed by Cramer [11]. An elastic analysis for a bolted timber butt joint was developed. The deformation of bolts against the wood and the deformation of the bolts against the steel plate were included in the model. It was shown that each bolt carries a different load if placed in a row. Stiffness-based approaches (like Wilkinson work [15]) build directly on the Cramer model, but introduced two main extensions: unequal fastener spacing and independent, piecewise linear-elastic displacement behaviour for each fastener, incorporating an initial slip. Based on these studies, for multiple fasteners in a row, the common

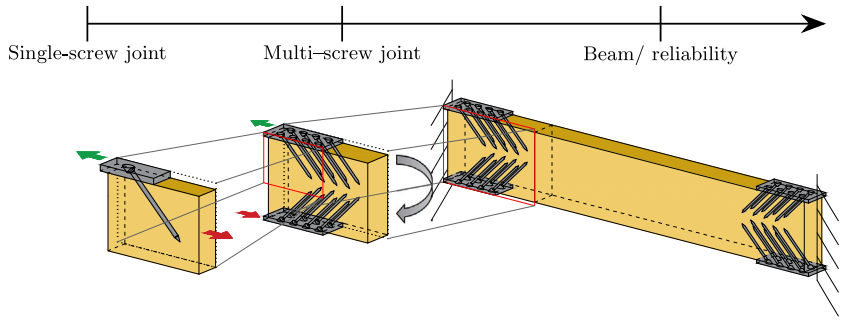


**Fig. 1.** Illustration of the applied multi-level probabilistic framework. Output from the single-screw model is used in the multi-screw joint model, which then informs the reliability analysis of the beam.

design approach was to apply a reduction factor (group action factor) to the sum of single-fastener capacity. Jorissen [14] tested double shear single and multi-bolt timber-to-timber joints and derived the effective number of fasteners as a function of the spacing and timber density. Research on multi-fastener timber joints continued to refine analytical models and extend them to new contexts. One area of interest is joints full load–displacement behaviour (not just the load-carrying capacity). The approaches involve the use of numerical 3D, 2D models and semi-analytical models. An overview of the possible 3D and 2D models is given in [16].

In 3D FEM, the contact between the fastener and the wood is modelled through a surface-to-surface contact with a penalty. Convergence issues at large displacements limit the applicability of these models. In 2D FEM, single-fastener joints are usually idealised as linear or nonlinear spring elements and then assembled, and their load–displacement curves, obtained from experiments, empirical or numerical models, must be used as inputs to the model. In the semi-analytical models approach, the fasteners are modelled with nonlinear springs and the load–displacement curve of each fastener is needed as input to the model. The local deformation of the wood between the fasteners is neglected, and an incremental loading procedure is required to obtain the whole load–displacement curve [17,18].

The semi-analytical approach avoids assembling a global stiffness matrix, drastically reducing computational time, and it neglects only minor elastic deformations in the wood (effects that are negligible beyond the initial loading stage [19]), making it well-suited for probabilistic failure analysis. Reliability analysis of statically indeterminate timber beams requires the derivation of the joint moment–rotation curve. The moment–rotation curve can be obtained through testing, analytical models, and the component-based method [20]. The component-based method is well established for the case of steel joints [21]. While timber design codes do not provide any design guidance, its effectiveness led researchers to adapt it to timber joints [20]. Based on the component method, the joint is idealised as an assembly of springs, representing a distinct mechanical part of the joints (such as timber in compression, a group of fasteners, steel plates, etc.). These springs are then assembled in parallel or series [22–25]. The method can be used to obtain the nonlinear moment–rotation curve, modelling the springs with nonlinear load-deformation curves [26]. Defining the nonlinear joint behaviour is essential, as these nonlinearities directly influence the reliability of timber structures. This is further motivated by previous studies explained in Section 1.3.

### *1.3. State of the art: impact of joints on the reliability of timber structures*

During recent years, researchers increasingly recognised that the semi-rigid, nonlinear behaviour of timber joints can significantly impact the reliability of timber structures [8,27–30]. Hansson [27] integrated the nonlinear behaviour of nailed joints with punched metal plates into reliability analyses of timber trusses. System effects and the impact of assumptions on the boundary conditions of the structures were assessed on the probability of failure. The results showed that for the studied truss the capacity calculated with reliability analysis exceeded the deterministic one, due to system effects. Kirkegaard [28] investigated the robustness of timber structures with respect to the ductile behaviour of the joints and the timber material, modelling the structure as a parallel system. It was found that even a small ductility increases the reliability of the structural system. Brühl [29], studied the impact of ductility and the overstrength factor on a statically indeterminate structure with dowelled joints. It was demonstrated that it is possible to get plastic redistribution in the structure if the requirements on the joints, not only in terms of resistance but also in terms of stiffness and ductility, are met. Recommendations on the right overstrength factor were given for the case of dowelled joints. Schilling [30] computed the impact of the nonlinear behaviour of dowelled timber joints with slotted-in steel plate on the reliability of timber trusses. It was shown that modelling these joints as fully pinned or clamped masks their semi-rigid, coupled behaviour, decreasing truss-level reliability and leading to potentially unsafe design. Caprio [8], used an elastic-perfectly plastic behaviour of joints as input in reliability analysis of statically indeterminate structures. The outcomes highlighted the importance of accounting for nonlinearities and the variability of joint behaviour for the reliability analyses of timber structures. Other researchers studied the effect of nonlinearities of the mechanical behaviour of timber joints on the deterministic analyses of structures [17,31,32]. Flatscher [31] integrated the nonlinear curve of hold-downs and angle brackets with self-tapping screws into a structural model of CLT walls under lateral loads. Klasson [32], studied the problem of the initial slip in the joints between the bracing system (purlins) and the main load-carrying members of timber roofs. It was found that slip in bracing members leads to higher stresses in the beams and lateral displacements. Schweigler [17] incorporated the nonlinear behaviour of a moment–rotation curve of multi-dowel joints into the nonlinear analyses of statically indeterminate timber structures. The nonlinear displacement curve of the dowelled joints with slotted-in plates affects the load distribution inside the structure. Therefore, Schweigler proposed the use of the mean value of stiffness in structural analysis with nonlinear joints.

Despite studies demonstrating the importance of incorporating joint nonlinearity into reliability and structural analyses, it remains unclear whether current design codes adequately capture these effects. This uncertainty is especially critical in statically indeterminate systems, where joint behaviour assumptions strongly influence the reliability. Beyond Eurocode stiffness reduction factor, nonlinear joint behaviour is typically considered using semi-analytical methods or FEM. The multi-level probabilistic framework proposed herein uses an empirical-probabilistic joint model to calibrate stiffness factors for direct use in design and efficient reliability analyses. This approach is more computationally efficient than nonlinear FEM, which is impractical for reliability studies with $\approx 10^6$ Monte Carlo simulation realisations due to excessive computation, but more accurate than simply applying current EC5 reduction factor, which might be inadequate for modern timber joints. This is the first study to assess the reliability of indeterminate timber beams with steel-to-timber joints and self-tapping screws, considering uncertainties in joints, loads, and timber. The output of the

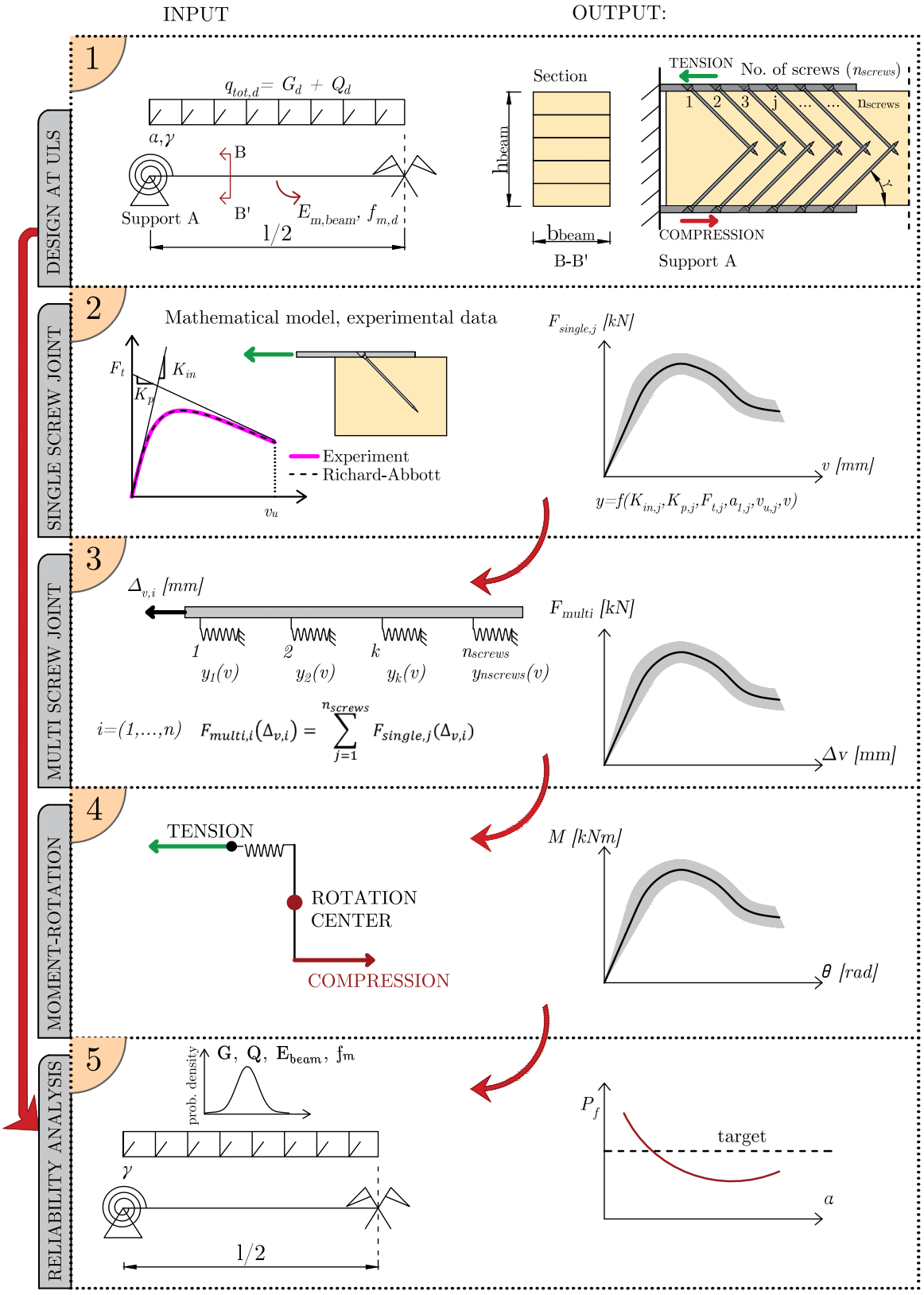


**Fig. 2.** Overview of the methodology.

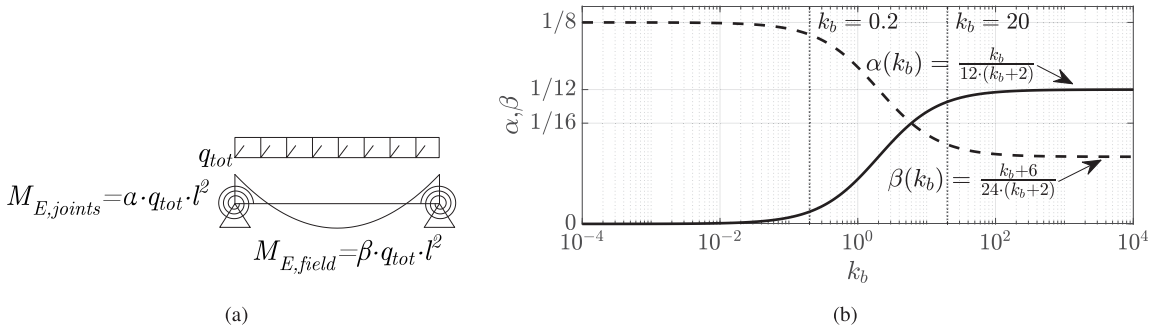


**Fig. 3.** Structure and load distribution: (a) Beam with semi-rigid joints under uniformly distributed load, (b) Load distribution according to $k_b$.

empirical single-screw model serves as input to the semi-analytical multi-screw model, from which the moment–rotation curves of multi-screw joints are derived for reliability analysis. The $K_{ULS}/K_{SLS}$ ratio is then calibrated to achieve target reliability. The developed multi-level framework is shown in Fig. 1. The work focuses on the bending performance of the structure, as it is the dominant failure for the given geometry and loads. The inclusion of other failure modes (e.g. shear, brittle failure) is left for future work. Section 2 details the models and their assumptions; Section 3 presents the multi-screw results, reliability analysis of the structures, and calibration of the design ratio; Section 4 summarises the conclusions and outlines possible future research.

## 2. Materials and methods

The methodology used herein to quantify the impact of the load–displacement curve of steel-to-timber joints with screws (characterised by different load-to-screw axis angles) on the reliability analysis of the statically indeterminate beam follows 5 steps:

1. Design of the structure according to EC5.
2. Generation of random load–displacement curves for single-screw joints.
3. Generation of the random load–displacement curve for multi-screw joints.
4. Derivation of the moment–rotation curve of joints.
5. Determination of the reliability of the entire structure and calibration of the ratio $K_{ULS}/K_{SLS}$.

An overview of the steps is illustrated in Fig. 2. Shear force is carried by a dedicated web joint, so shear and bending follow separate load paths at the joints. For the geometry and loading considered here, shear demand is assumed below the beam and joints capacity, making bending the governing failure mode and the focus of the present reliability analysis. The interpretation of the load-to-screw axis angle ($\gamma$) is illustrated in Fig. 2.

### 2.1. Design of a statically indeterminate structure

The simplest example of a statically indeterminate structure is a statically indeterminate timber beam (Fig. 3(a)). The effect of joint stiffness on moment distribution can be illustrated by the example in Fig. 3(a). The support and midspan moments are written as a function of the coefficients $\alpha$ and $\beta$, which depend on the rotational stiffness of the joints and on the bending stiffness of the beam [33], as follows:

$$\alpha = \frac{K_{\theta,joints}\cdot l}{24\cdot E_{m,beam}\cdot I_{beam}+12\cdot K_{\theta,joints}\cdot l} \text{ and } \beta=\frac{1}{8}-\alpha. \tag{1}$$

Where $K_{\theta,joints}$ is the rotational stiffness of the joins, $l$ is the beam span, $E_{m,beam}$ and $I_{beam}$ are the mean elastic stiffness and the bending moment of inertia of the beam, respectively. Intuitively, $\alpha$ measures how 'rigid' the joint is compared to the bending stiffness of the connected member over a span: when $\alpha \to 0$, the joint is defined as ideally pinned (zero moments at joints), while when $\alpha \to 0.0833$ (1/12) the joint is considered as ideally clamped (moment distribution close to the rigid-joint limit). Joints can be classified into pinned, semi-rigid or clamped according to the bending dimensionless stiffness ratio, as it is currently done in EC3 [21]: $k_b = (K_{\theta,joints}\cdot l)/(E_{m,beam}\cdot I_{beam})$. The parameters $\alpha$ and $k_b$ are both relative stiffness factors, but $\alpha$ is bounded and acts as a moment-allocation coefficient. The expression for $\alpha$ also depends on the type of applied loads, such as a uniformly distributed load.

Fig. 3(b) (adapted from [34]) identifies three joint-behaviour regions based on the dimensionless stiffness parameter $k_b$: pinned ($k_b < 0.2$), semi-rigid ($0.2 \le k_b \le 20$), and clamped ($k_b > 20$). Using a 10% error criterion on $\alpha$, $|\alpha(k_b) - (1/12)|/(1/12) < 0.10$ for the upper limit, and at lower bound end (where division by zero is undefined) the absolute bound $\alpha(k_b) < 0.10$, the semi-rigid range shows that the bending moment in the beam still varies with joint stiffness, whereas $k_b \le 0.2$ and $k_b \ge 20$ further changes in stiffness alter the moment by less than 10%, so the joints can be considered effectively pinned ($k_b \le 0.2, \alpha \le 0.01$) or clamped ($k_b \ge 20, \alpha \ge 0.075$).

Although the design could follow numerous approaches, for the sake of simplifying two representative ones are chosen: the stiffness-based approach and the capacity-based approach. The flowchart of both strategies is represented in Fig. 4. The stiffness-based design strategy (summarised in Fig. 4(a)) consists of five design steps plus one side input for the joint lateral properties:

1. *Assignment of a rigidity level:* $\alpha = (0, \dots, 0.0833)$.
2. *Computation design bending moments:* using the selected $\alpha$, the acting moments at the joints $M_{Ed,joints}$ and midspan $M_{Ed,field}$ are calculated:

$$M_{Ed,joints} = \alpha \cdot q_{tot,d}\cdot l^2, \qquad M_{Ed,field} = \beta\, q_{tot,d}\cdot l^2 \tag{2}$$

   Where $q_{d,tot}$ is the design value of the distributed load.
3. *Calculation of the beam section:* $b_{beam}$ is fixed to 165 mm. The beam height is calculated as follows:

$$h_{beam} = \sqrt{\frac{6\cdot \max\left(M_{Ed,joints}, M_{Ed,field}\right)}{b_{beam}\, f_{m,d}}} \tag{3}$$

   with $f_{m,d}$ the design bending strength of glulam.
4. *Check of the joint rotational stiffness at ULS:* the joints target stiffness is:

$$K_{\theta,d,ULS,joints} = \frac{24\cdot E_{m,beam}\cdot I_{beam}\cdot \alpha}{l_{beam}\cdot(1-12\cdot\alpha)} \tag{4}$$

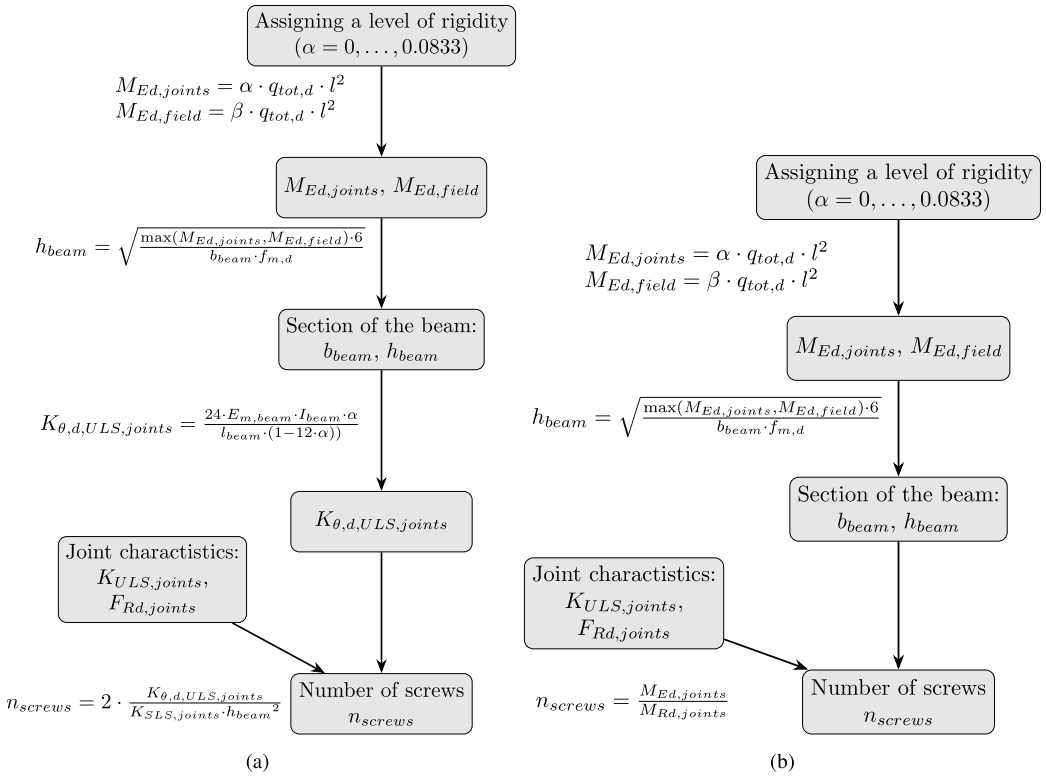


**Fig. 4.** (a) Stiffness-based design approach, (b) Capacity-based design approach.

5. *Determination of the number of screws:* assuming the neutral axis at the middle of the beam height, the total number of screws in the tension side can be calculated as:

$$n_{screws} = \frac{K_{\theta,d,ULS,joints}}{K_{\theta,ULS,joints}} = \frac{K_{\theta,d,ULS,joints}}{K_{ULS,joints} \cdot z^2} = 2 \cdot \frac{K_{\theta,d,ULS,joints}}{K_{ULS,joints} \cdot h_{beam}^2} \tag{5}$$

$n_{screws}$ is rounded up to the next even integer. $K_{ULS,joints}$ is the lateral stiffness at ULS of single-screw joints, $K_{\theta,ULS,joints}$ is the rotational stiffness of single-screw joints, and $z$ is the level arm, that in this case is equal to $h_{beam}/2$. $K_{\theta,ULS,joints}$ is calculated as:

$$K_{\theta,ULS,joints} = n_{screws} \cdot K_{ULS,joints} \cdot z^2 \tag{6}$$

The capacity-based design strategy is illustrated in Fig. 4(b). The design steps up to 3rd are the same, however, $n_{screws}$ is instead selected based on the capacity: $n_{\text{screws}} = M_{Ed,joints}/M_{Rd,joints}$. $M_{Ed,joints}$ and $M_{Rd,joints}$ are the moment acting at the joints and the bending capacity of the joints.

### 2.2. Empirical-probabilistic model of single screw-joints

The model of the single-screw joints is based on the data from the experimental campaign reported in [35,36], where an empirical-probabilistic model was developed as a function of different values of load-to-screw axis angle. Four linear variable displacement transformers (LVDTs) were installed. Two LVDTs were mounted at the top and bottom of the steel plate to monitor out-of-plane movement (perpendicular to the shear plane); the relative data were not analysed. The relative displacement between the steel plate and the timber specimen at the joints was recorded by two LVDTs placed on opposite sides of the specimen, and only these data were used in the analysis. The load was measured by an electric load cell (220 kN capacity) in the testing machine. The tests were performed taking the EN 12512 [37] as a reference, but always in a displacement-controlled mode with a speed of 1 mm/min. The test set-up is illustrated in Fig. 5, while the material, and geometric properties of components in Table 1. The test matrix and observed failure modes are shown in Table 2.

**Table 1**
Geometrical and mechanical characteristics of the screws, timber and steel plate.

| | |
|---|---|
| Screws[a] | $d = 8mm$; $l_{eff} = 200$ $mm$; $d_{core} = 5.1$ $mm$ |
| Timber[b] | GL30c; MC $11.6 \pm 1\%$ |
| Plate | S355, $t_{plate} = 15$ $mm$; $l_{plate} = 319$ $mm$: $b_{plate} = 89$ $mm$ |

*$d$ nominal diameter; $l_{eff}$ effective length; $d_{core}$ core diameter, $MC$ moisture content.

**Table 2**
Test matrix and corresponding failure mode.

| $\gamma$ [°] | $n_{tot}$ | $n_{HTO}$ | $n_{WITH}$ |
|---|---|---|---|
| 30 | 10 | 4 | 6 |
| 45 | 20 | 18 | 2 |
| 60 | 10 | 10 | 0 |
| 90 | 20 | 20 | 0 |

$n_{tot}$ total No. of tests; $n_{HTO}$ No. head tear-off failures; $n_{WITH}$ No. withdrawal failures.

The single-screw joint load–displacement curve using the Richard-Abbott [38] model was approximated as follows:

$$F_{single} = \begin{cases} \dfrac{(K_{in} - K_p) \cdot v}{(1 + (\frac{(K_{in} - K_p)}{F_t} \cdot v)^{a_1})^{\frac{1}{a_1}}} + K_p \cdot v, & v_{in,shift} < v < v_u \\ 0, & v < v_{in,shift} \end{cases} \tag{7}$$

Where $K_{in}$, $F_t$, $K_p$ and $a_1$ are the parameters of the Richard-Abbott model. The initial slip $v_{in,shift}$ is defined as a region of low or "zero stiffness", at very low load levels, due to (i) tolerances/clearance between fastener and hole that delay contact, and (ii) embedment of timber

**Table 3**
Overview of Richard-Abbott model parameters by angle: unit, distribution, mean value and CoV.

| | | | $\gamma$ [°] | | | | | | | |
|---|---|---|---|---|---|---|---|---|---|---|
| | | | 30 | | 45 | | 60 | | 90 | |
| Input | Unit | Distribution | Mean V. | COV | Mean V. | COV | Mean V. | COV | Mean V. | COV |
| $K_{in}$ | kN/mm | Lognormal | 18.35 | 0.21 | 16.24 | 0.14 | 8.84 | 0.10 | 1.63 | 0.32 |
| $F_1$ | kN | Lognormal | 35.10 | 0.06 | 38.25 | 0.24 | 39.80 | 0.25 | 2.75 | 0.75 |
| $K_p$ | kN/mm | Normal | −4.10 | 0.14 | −4.90 | 0.56 | −3.64 | 0.37 | 0.76 | 0.20 |
| $a_1$ | – | Lognormal | 8.10 | 0.53 | 5.00 | 0.31 | 4.19 | 0.29 | 7.26 | 0.58 |
| $v_u$ | mm | Lognormal | 2.53 | 0.07 | 2.97 | 0.13 | 4.47 | 0.10 | 13.85 | 0.16 |

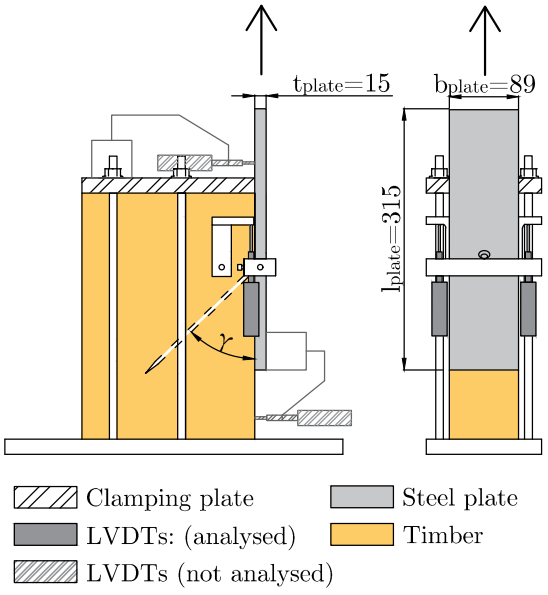


**Fig. 5.** Test setup for the single-screw joint tests [36].

under the loaded fastener. The effect is more pronounced when using washers or very oversized holes, and smaller for milled holes. $v_{in,shift}$ is assumed equal to a random realisation from the uniform distribution $\mathcal{U}$ over the 1 mm hole-clearance tolerance, i.e. $v_{in,shift} \sim \mathcal{U}(0, +1\ mm)$. $v_u$ is the ultimate displacement in correspondence with the head-tear off failure of the screw. The mean values and the COVs of the model parameters for each load-to-screw axis angle are given in Table 3.

For the load-to-screw axis angle of 30° and 45°, both head tear-off failure and withdrawal failure of the screw occurred. The load–displacement curves presented different characteristics: head-tear off failure of the screw resulted in a drop in load at the failure point, while withdrawal failure of the screw resulted in a softening post-peak behaviour. Therefore, the random curves are generated reflecting the probability of occurrence of a failure mode, calculated as: $P_{HTO} = \frac{n_{HTO}}{n_{tot}}$, $P_{WITH} = 1 - P_{HTO}$.

Where $P_{HTO}$ is the probability of occurrence of the head-tear off failure, $P_{WITH}$ is the probability of occurrence of the withdrawal failure. For joints with screws with load-to-screw axis angle of 30°, $P_{HTO}$ = 60%, $P_{WITH}$ = 40%. For the angle 45°, $P_{HTO}$ = 90% and $P_{WITH}$ = 10%. For the angles of 60° and 90°, $P_{HTO}$ = 100%. Since the variability of the parameters in case of withdrawal failure of the screws cannot be reliably determined, the load–displacement curve and its variability are assumed identical to those of head tear-off, with the sole modification that the curve is extended until the load decreases to zero rather than truncated at the ultimate displacement $v_u$.

### 2.3. Model of multi-screw joints

After obtaining the load–displacement curves of a single-screw joints, this data is used as input in the model for the multi-screw joint. According to the empirical-probabilistic model of the single-fastener joint, an individual load–displacement curve is generated for each screw. In the multi-screw model, these curves are combined to represent the behaviour of the entire multi-screw joint. The model is based on the following assumptions: (i) timber is assumed to be rigid, thus, the deformations between the screws are neglected; (ii) steel plates are assumed to be rigid. Thus, the screws are subjected to the same axial and lateral deformation.

Following these assumptions, the force $F_{single,j}$ at the specific displacement value $\Delta_{v,i}$ is obtained for every screw. The sum of these forces resulted in the force of the entire joint $F_{multi,i}$ at that displacement increment:

$$F_{multi,i}(\Delta_{v,i}) = \sum_{j \in \mathcal{A}} F_{single,j}(\Delta_{v,i}), \qquad (i = 1, \dots, n) \tag{8}$$

$\mathcal{A}$ is the active set of screws and $n$ is the number of displacement increments. As displacement increases, any screw exceeding its ultimate slip ($v_{u,j}$) is removed from $\mathcal{A}$, and the process continues until all screws have failed. If the single screw joint is characterised by brittle failure, this produces a brittle, sudden loss of capacity (drop) in the curve of the multi-screw joint. The procedure is summarised as follows:

1. *Inputs:* single–screw load–displacement curves for $j = 1, \dots, n_{screws}$, $F_{single,j}(\Delta v)$ defined for $\Delta v \in [0, v_{u,j}]$; displacement increment $\Delta v_{inc} = 0.2$ mm. The first displacement increment is $\Delta_{v,1} = 0$ and the set of active screws $\mathcal{A} = \{1, \dots, n_{screws}\}$.
2. At each step: the new value of displacement is increased: $\Delta_{v,i} = \Delta_{v,i-1} + \Delta_{v,inc}$. and the multi-screw force is calculated according to Eq. (8).
3. Failure check: if any $j \in \mathcal{A}$ has $\Delta_{v,i} > v_{u,j}$, the screw is removed from the active group of screws: $\mathcal{A} \longleftarrow \mathcal{A} \setminus \{j\}$.

The process is increased until no active screw remains $\mathcal{A} = \varnothing$. The probabilistic, displacement-controlled multi-screw joint model captures the change that occurs in the load–displacement curve as fasteners fail (one less spring in parallel). However, it does not account for interaction effects that depend on the spacing between screws, nor re-distribution effects. This is justified assuming that in the adopted design, the screws are arranged using spacing well above code-specified distances (EC5), so that the interaction of screws does not occur. These assumptions help isolate the influence of nonlinear joint stiffness on system reliability.

### 2.4. Moment–rotation model of joints via the component method

Once the model of the multi-screw joints is established, the entire moment–rotation behaviour of the joint is obtained via the component method.

The tension force is carried by a joint positioned on the tension side of the neutral axis, while the compression is carried by another joint located on the compression side of the neutral axis. The centre of rotation coincides with the centre of beam height, and the lever arm is $z = h_{beam}/2$ and the couple arm $s = h_{beam}$. The bending moment and the rotation with multi-screw can be written as:

$$M_{R,joints,i} = F_{multi,i} \cdot s, \tag{9}$$

$$\theta_i = \frac{\Delta_{v,i}}{z}, \quad (i = 1, \dots, n) \tag{10}$$

$F_{multi,i}$ is the force in the multi-screw joints at the $i$th displacement increment and $n$ is the total number of displacement increments. In this model, the compression-side joint supplies the counter-resultant. Since $s$ and $z$ are constant parameters, the shape of the $M_{R,joints} - \theta$ curve matches the tension-side multi-screw curve, differing only by a scale factor.

### 2.5. Reliability analysis of the structure

A structural reliability analysis aims to determine the probability of failure of a system according to one or more failure modes in the presence of different uncertainties. Each one of the failure modes can be defined by a limit-state equation $g(\mathbf{X})$ (also called performance function), expressed as follows:

$$g(\mathbf{X}) = R(\mathbf{X}) - E(\mathbf{X}) \tag{11}$$

Where $R(\mathbf{X})$ is the capacity, and $E(\mathbf{X})$ is the demand. Both capacity and demand depend on the vector of random variables $\mathbf{X}$. The failure is reached when the $E$ exceeds $R$: $g(\mathbf{X}) \leq 0$. The probability of failure $P_f$ is defined as follows according to [39,40]:

$$P_f = \int_{D_f} f_{\mathbf{X}}(\mathbf{x}) d\mathbf{x} \tag{12}$$

Where $f_{\mathbf{X}}()$ is the probability density function of the vector of random variables $\mathbf{X}$ and $D_f$ is the failure domain. No closed-form expression for multi-dimensional, non-Gaussian structural reliability problems can be found for Eq. (12) [41], which leads to the use of approximation methods, simulation methods or adaptive surrogate-modelling-based methods. In this paper, a crude MCS is used to compute the $P_f$ of the structure. In a previous study, MCS proved to be the most convenient method in terms of accuracy for computing the reliability of statically indeterminate timber beams [8].

When dealing with statically indeterminate structures, a single performance function cannot capture all possible failure modes. Joints introduce additional complexity: the structure may fail in the timber at midspan, at a joint, or the joints themselves may fail. Each of these failure mechanisms requires its own limit-state equation [8].

Preliminary design checks indicate that bending failure governs the design for long-span beams, while shear is not critical. Accordingly, the present study focuses on bending failure as the critical performance function. Although in reality the bending strength varies along the beam length and failure may occur at various locations, in this study, the bending strength is considered constant along the beam length. Hence, bending failure occurs where the moment envelope has its maximum. For a beam with semi-rigid joints, those peaks are at midspan and/or the joints sections depending on the joint rigidity, so these locations govern the reliability analysis. The bending failure at midspan happens when $g_1 \leq 0$, where $g_1$ is the following performance function:

$$g_1(\mathbf{X}) = M_{R,beam}(\mathbf{X}) - M_{E,field}(\mathbf{X}) \tag{13}$$

Failure happens in the timber at the joints when $g_2 \leq 0$, where $g_2$ is the following performance function:

$$g_2(\mathbf{X}) = M_{R,beam}(\mathbf{X}) - M_{E,joints}(\mathbf{X}) \tag{14}$$

$\mathbf{X}$ is the vector of random variables, $M_{R,beam}(\mathbf{X})$ is the bending capacity of the beam, $M_{E,joints}(\mathbf{X})$ and $M_{E,field}(\mathbf{X})$ are the moment acting at the joints and midspan, respectively.

In case the beam is strong enough to prevent initial bending failure, the joint itself will be loaded. Subsequently, the load is redistributed along the beam. Finally, suppose the rotation capacity of the joints is exceeded. In that case, the structural system becomes a simply supported beam, whose failure happens when $g_3 \leq 0$. $g_3$ is defined as follows:

$$g_3(\mathbf{X}) = \max(g_{3.1}(\mathbf{X}), g_{3.2}(\mathbf{X})) \tag{15}$$

$g_{3.1}$ represents the joints ultimate rotation performance function and $g_{3.2}$ represents the simply supported beam performance function:

$$g_{3.1}(\mathbf{X}) = \theta_u(\mathbf{X}) - \theta_{req}(\mathbf{X}), \quad g_{3.2}(\mathbf{X}) = M_{R,\text{beam}}(\mathbf{X}) - M_{max}(\mathbf{X}) \tag{16}$$

$\theta_u$ is the ultimate rotation of joints and $\theta_{req}$ is the required rotation at the joints. $\theta_{req}$ is:

$$\theta_{req} = \frac{q_{tot} \cdot l^3}{24 \cdot E_{beam} \cdot I_{beam}} - \frac{M_{E,joints} \cdot l}{2 \cdot E_{beam} \cdot I_{beam}} \tag{17}$$

$M_{max}$ is equal to $\frac{1}{8} \cdot q_{tot} \cdot l^2$, the maximum moment at midspan of a simply supported beam. For certain design situations, reaching the ultimate rotation of joints implies failure of the entire structure. In this case, $g_3$ simply becomes $g_{3.1}$. The total probability of failure $P_f$ is the union of the three failure probabilities. Since these three performance functions are mutually exclusive, $P_f$ is the sum of the single failure probabilities, as follows:

$$P_f = P[g_1 \leq 0 \cup g_2 \leq 0 \cup g_3 \leq 0] = P[g_1 \leq 0] + P[g_2 \leq 0] + P[g_3 \leq 0] \tag{18}$$

In order to find $M_{E,joints}(\mathbf{X})$ and $M_{E,field}(\mathbf{X})$, the beam-line method is used. The beam-line method was initially developed for steel structures [42] and then applied to timber structures [29,43]. The equation of the beam line is the following:

$$M^j_{E,joints} = \frac{2}{3} \cdot M^j_{max} \cdot \left(1 - \frac{\theta^j}{\theta^j_{max}}\right) \tag{19}$$

Where $M^j_{max}$ and $\theta^j_{max}$ are the moment and the rotation in a simply supported beam at midspan, in correspondence of the $j$th load increment $\Delta_j$, respectively. $\theta^j$ is the rotation at the joints at equilibrium corresponding to that same load increment. When the moment at the joints is equal to $2/3 \cdot M_{max}$ and the rotation at the joints is zero, the system is a fully clamped beam. When the rotation at the joints is equal to $\theta_{max}$ and the moment at the joints is zero, the structural system instead represents a simply supported beam.

The graphical representation of this incremental loading procedure is illustrated in Fig. 6. At each load increment, the intersection between Eq. (19) and the moment–rotation curve of the joints can be calculated. The intersection represents the equilibrium moment at the joints $M^j_{E,joints}$ for that load increment. The moment at midspan $M^j_{E,field}$ can then be calculated as $M^j_{max} - M^j_{E,joints}$. The load can be increased incrementally until one of the performance functions (Eq. (13)-Eq. (16)) becomes negative or until the load reaches the (final) realisation of the value $q_{t,tot}$. Fig. 6(a) illustrates the case when, at a certain load increment, the failure is reached at midspan, i.e. $M^t_{R,beam}$ is exceeded (red zone in the Figure). Fig. 6(b) represents the case when $M^t_{R,beam}$ is reached at the joints instead. Finally, Fig. 6(c) illustrates the case where the load is increased until the final value $q_{t,tot}$, but no failure happens, neither at midspan nor at the joint, i.e. the structure resists the applied load.

Because the analysis uses the beam-line method, the joints rotation capacity is not verified directly with $g_{3.1}$. If no intersection is found, the required rotation exceeds the ultimate rotation of joints. In this case, the structure is evaluated as a simply supported beam. The input variables used in the reliability analysis are given in Table 4.

Both parameter–parameter and parameter–material property correlations are reported in Table 5. The correlation $\rho_{(P_{mod,k},\rho_{den})}$ between each parameters of the model $P_{mod,k}$ and the density of the lamellas $\rho_{den}$ in which the screw was embedded is calculated, based on experimental measured densities. Due to a limited data on load–displacement curve of the single-screw joint [36], the $\rho_{(P_{mod,k},rho_{dens})}$ are subjected to uncertainty. Therefore, the level of correlation has to be intended as approximate. Because the bending strength $f_m$ and elastic stiffness $E_{beam}$ strongly depend on density $\rho_{den}$, the missing correlations are estimated via the single-factor product rule [45]:

$$\begin{aligned} \rho_{(P_{mod,k},f_m)} &= \rho_{(P_{mod,k},\rho_{den})} \cdot \rho_{(\rho_{den},f_m)}, \\ \rho_{(P_{mod,k},E_{beam})} &= \rho_{(P_{mod,k},\rho_{den})} \cdot \rho_{(\rho_{den},E_{beam})}. \end{aligned} \tag{20}$$

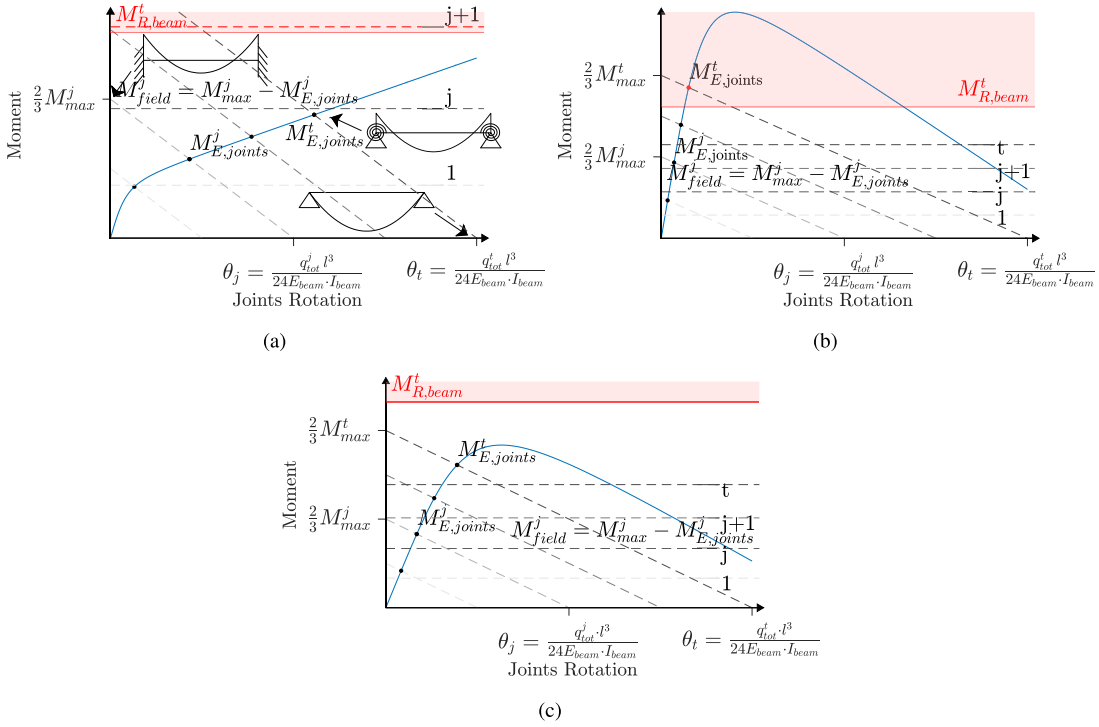


**Fig. 6.** Beam line method for different cases: (a) failure at midspan, (b) failure at the joints, (c) no failure.

**Table 4**
Overview of loads a and material properties parameters by angle: unit, distribution, mean and characteristic value and COV.

| Input variable | Unit | Distribution | Char V. | Mean V. | COV |
|---|---|---|---|---|---|
| $G^*$ | $\frac{kN}{m}$ | Normal | – | 0.65 | 0.1 |
| $Q^*$ | $\frac{kN}{m}$ | Gumbel | 5.85 | 3.21 | 0.3 |
| $f_m^*$ | $\frac{N}{mm^2}$ | Lognormal | 30 | 38.8 | 0.15 |
| $E_{beam}^*$ | $\frac{N}{mm^2}$ | Lognormal | – | 13′000 | 0.13 |
| $W_{el}$ | $m^{-3}$ | Constant | Design based | | – |
| $l$ | $m$ | Constant | – | 10 | – |

(*) Based on the indication contained in JCSS [44].

Thus, each correlation between the material properties and the model parameters is taken as the product of the correlation between the model parameters and the density and the correlation between the density and the material property. The available correlation matrix is defined for material properties $\mathbf{Y} = (E_{beam}, f_m)$ and the curve parameters $\mathbf{P}_{\text{mod}} = (P_{mod,1}, \dots, P_{mod,m})$ of a single-screw joint. In the MCS, each joint contains $n_{screws}$ screws, so the parameters vector $\mathbf{P_{mod}}$ has to be generated $n_{screws}$ times per each MCS run. For each screw $j = 1, \dots, n_{screws}$ that composes the multi-screw joint, given the material property vector $\mathbf{Y} = (E_{beam}, f_m)$, each vector of $\mathbf{P}_{\text{mod}}^{(j)} = (P_{mod,1}^{(j)}, \dots, P_{mod,m}^{(j)})$ is sampled conditionally as follows:

1. *Material properties:* once per run $\mathbf{Y} \leftarrow \mathcal{N}_2(0, \Sigma_{\mathbf{YY}})$ is sampled, and the two latent normals are transformed to the corresponding lognormal.
2. *Parameters of the single-screw joint:* for each screw $j = 1, \dots, n_{screws}$ that composes the multi-screw joint:

$$\mathbf{P}_{mod}^{(j)} \,\Big|\, \mathbf{Y} = y \sim \mathcal{N}_m\Big(\underbrace{\Sigma_{\mathbf{P}_{mod}^{(j)}\mathbf{Y}}\Sigma_{\mathbf{YY}}^{-1}y}_{\text{shifted mean}},\ \underbrace{\Sigma_{\mathbf{P}_{mod}^{(j)}\mathbf{P}_{mod}^{(j)}} - \Sigma_{\mathbf{P}_{mod}^{(j)}\mathbf{Y}}\Sigma_{\mathbf{YY}}^{-1}\Sigma_{\mathbf{YP}_{mod}^{(j)}}}_{\text{reduced covariance}}\Big) \tag{21}$$

where with this notation it is meant that the sampling is done with the conditional probability distribution of $\mathbf{P}_{mod}^{(j)}$ given $\mathbf{Y} = y$.

3. *Physical space:* finally, every component of $\mathbf{P}_{mod}^{(j)}$ is transformed from the latent normal to the corresponding lognormal.

## 3. Results and discussion

### 3.1. Design criteria of the structure

Satisfying the joint stiffness and load-carrying capacity requirements simultaneously is challenging. Not every degree of rigidity is feasible for joints with screws with the specific screw-to-grain angle. Feasible points are values of the degree of rigidity, $\alpha$, at which both of the following hold simultaneously: (i) the relative stiffness requirement is met $\alpha_d \geq \alpha$, (ii) The resistance requirement is met $M_{Rd,\text{joints}} \geq M_{Ed,\text{joints}}$. $\alpha_d$ is the value of $\alpha$ after the actual number of screws $n_{screws}$ is fixed in the design. The governing stiffness requirement must be the more restrictive of resistance or stiffness: if resistance governs, the actual joint stiffness will exceed the assumed $\alpha$, thereby altering $M_{Ed,joints}$; if stiffness governs, $M_{Ed,joints}$ remains as assumed, since the joint stiffness has been calibrated exactly to the target $\alpha$. In case a level of rigidity is not feasible, alternatively, different screws or different screw-to-grain angles should be chosen in that case. For joints with screws, the capacity requirement is almost always more stringent than the stiffness one for low and medium values of rigidity. The closer the joint is designed to be a clamped joint ($\alpha > 0.075$), the stricter the stiffness requirements become. Thus, to achieve a chosen degree of rigidity, the number of screws needed to satisfy the inequality $M_{Rd,joints} \geq M_{Ed,joints}$ is larger than the number of screws needed to satisfy the inequality $\alpha_d \geq \alpha$. This can be seen in Fig. 7, where the number of screws (vertical axis) in order to meet the stiffness and the capacity requirements is shown for the screw properties used in this paper.

Feasible solutions first appear at $\alpha \geq 0.077$ for joints with load-to-screw axis angle of 30° and 45° (Fig. 7(a)), at $\alpha \geq 0.074$ for joints with load-to-screw axis angle of 60°. For the joints with a load-to-screw axis angle of load-to-screw axis angle of 90°, every value of $\alpha$

**Table 5**
Correlation matrix of the regression parameters as a function of the load-to-screw axis angle.

| $\gamma$ | 30 ° | | | | | | 45 ° | | | | | |
|---|---|---|---|---|---|---|---|---|---|---|---|---|
| | $F_t$ | $K_p$ | $a_1$ | $v_u$ | $\rho_{den}$ | $E_{beam}, f_m$ [a] | $F_t$ | $K_p$ | $a_1$ | $v_u$ | $\rho_{den}$ | $E_{beam}, f_m$ [a] |
| $K_{in}$ | 0.72 | −0.72 | −0.85 | −0.77 | 0.40 | 0.20 | 0.42 | −0.49 | −0.43 | −0.71 | 0.40 | 0.20 |
| $F_t$ | 1.00 | −1.00 | −0.60 | −0.47 | 0.40 | 0.20 | 1.00 | −0.99 | −0.81 | −0.15 | 0.20 | 0.00 |
| $K_p$ | | 1.00 | 0.60 | 0.47 | −0.40 | −0.20 | | 1.00 | 0.80 | 0.19 | −0.20 | 0.00 |
| $a_1$ | | | 1.00 | 0.46 | −0.20 | 0.00 | | | 1.00 | −0.07 | −0.20 | 0.00 |
| $v_u$ | | | | 1.00 | −0.20 | 0.00 | | | | 1.00 | −0.20 | 0.00 |
| $\rho_{den}$ | | | | | 1.00 | 0.60 | | | | | 1.00 | 0.60 |
| $E_{beam}, f_m$ | | | | | | 1.00 | | | | | | 1.00 |

| $\gamma$ | 60° | | | | | | 90° | | | | | |
|---|---|---|---|---|---|---|---|---|---|---|---|---|
| | $F_t$ | $K_p$ | $a_1$ | $v_u$ | $\rho_{den}$ | $E_{beam}, f_m$ [a] | $F_t$ | $K_p$ | $a_1$ | $v_u$ | $\rho_{den}$ | $E_{beam}, f_m$ [a] |
| $K_{in}$ | −0.25 | 0.26 | 0.14 | −0.79 | 0.40 | 0.20 | 0.10 | 0.28 | −0.19 | −0.50 | −0.40 | −0.20 |
| $F_t$ | 1.00 | −0.95 | −0.93 | 0.60 | 0.20 | 0 | 1.00 | −0.75 | −0.40 | 0.10 | −0.20 | 0 |
| $K_p$ | | 1.00 | 0.86 | −0.48 | −0.20 | 0 | | 1.00 | 0.40 | −0.34 | 0.00 | 0 |
| $a_1$ | | | 1.00 | −0.51 | −0.20 | 0 | | | 1.00 | 0.02 | 0.00 | 0 |
| $v_u$ | | | | 1.00 | −0.40 | −0.40 | | | | 1.00 | 0.40 | 0.20 |
| $\rho_{den}$ | | | | | 1.00 | 0.60 | | | | | 1.00 | 0.60 |
| $E_{beam}, f_m$ | | | | | | 1.00 | | | | | | 1.00 |

[a] The correlation between $E_{beam}$ and $f_m$ is set to 0.8 as prescribed by JCSS [44].

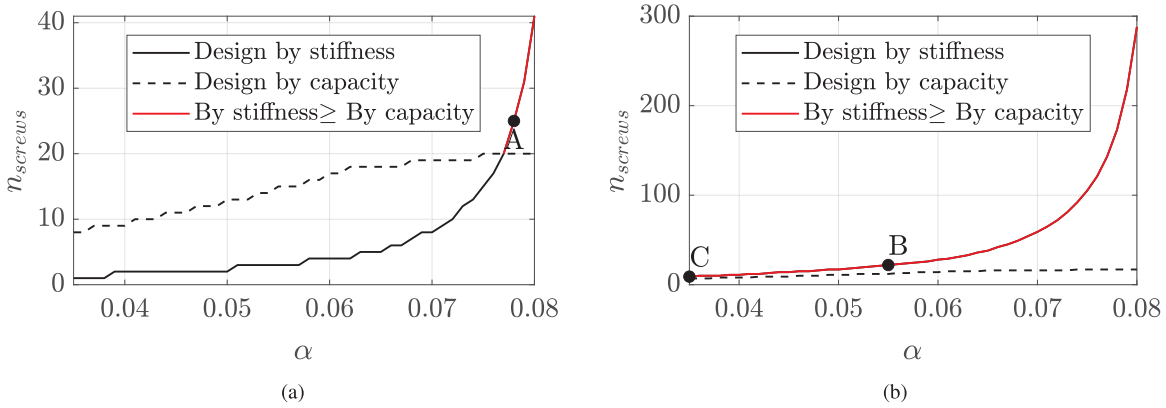


**Fig. 7.** Number of screws $n_{screws}$ required according to the stiffness-based design and resistance-based design approach for the joints with screws with a load-to-screw axis angle of (a) 45°, (b) 90°. The design parameters of points "A", "B", "C" are reported in Table 6.

is feasible. However, SLS requirements rule out very small $\alpha$, so for 90° the reliability analysis is restricted to $\alpha \geq 0.035$. Moreover, $\alpha = 0.08$ would demand roughly 300 screws in a single joint, so that point is kept only for completeness (Fig. 7(b)). Given the studied geometry ($b_{beam} = 165$ mm) and EC5 spacing/edge distances, achieving $\alpha \approx 0.067$ with screws at 90° requires about 45 screws splitted in three rows. Increasing $\alpha$ further by adding more screws is impractical due to space constraints, interactions, and the risk of brittle failure modes. Instead, designers use inclined screws, which provide higher stiffness and reach the same $\alpha$ with fewer screws. A summary of design parameters for representative cases is reported in Table 6. Dimensions are given as continuous (non-standard) values, since rounding up to standard glulam sizes would artificially increase the reliability and make the computed $P_f$ fluctuate around the target. Design values of actions and materials are obtained using the partial safety-factor format of EC0 [46]. For timber, the material design rules follow EC5. Load-duration effects ($k_{mod}$) are neglected in the design because the governing ultimate limit state (ULS) combinations are of short duration. Moreover, the long-term effects are not modelled explicitly in the present reliability analysis. If $k_{\text{mod}}$ were applied, the target failure probability would be reduced, which in turn would require a more runs for MCS to achieve a reliable estimate of $P_f$, while the results of the reliability analysis would remain the same.

**Table 6**
Summary of design parameters for representative cases. $b_{beam} = 165$ mm, $G_k = 0.65$ kN, $Q_k = 5.85$ kN.

| Case | $\alpha$ | $h_{beam}$ [mm] | No. screws/row × No. rows | $\gamma$ [°] |
|---|---|---|---|---|
| A | 0.078 | 338 | 24 [8 × 3] | 45 |
| B | 0.035 | 363 | 9 [3 × 3] | 90 |
| C | 0.055 | 320 | 21 [7 × 3] | |

### 3.2. Multi-screw joints

In the multi-screw model, a load–displacement curve is generated for each joint by sampling from the randomly established single-screw curves according to the empirical probabilistic models described in Section 2.2. The resulting multi-screw joint behaviour can be analysed by computing three key parameters that describe the characteristics of the load–displacement curve: the elastic stiffness $K_{10-40}$, the load-carrying capacity $F_{max}$ and the absolute ductility $D_{ab}$.

The elastic stiffness is computed as the secant between two load levels, typically 10% and 40% of the load-carrying capacity, which also represents the SLS. The load-carrying capacity $F_{max}$ is the maximum force the joint can experience, and the ductility follows the absolute definition (see also [47]), i.e.: $D_{ab} = v_u - v_y$. Where $v_y$ is the displacement at the yielding point and $v_u$ is the ultimate displacement at failure

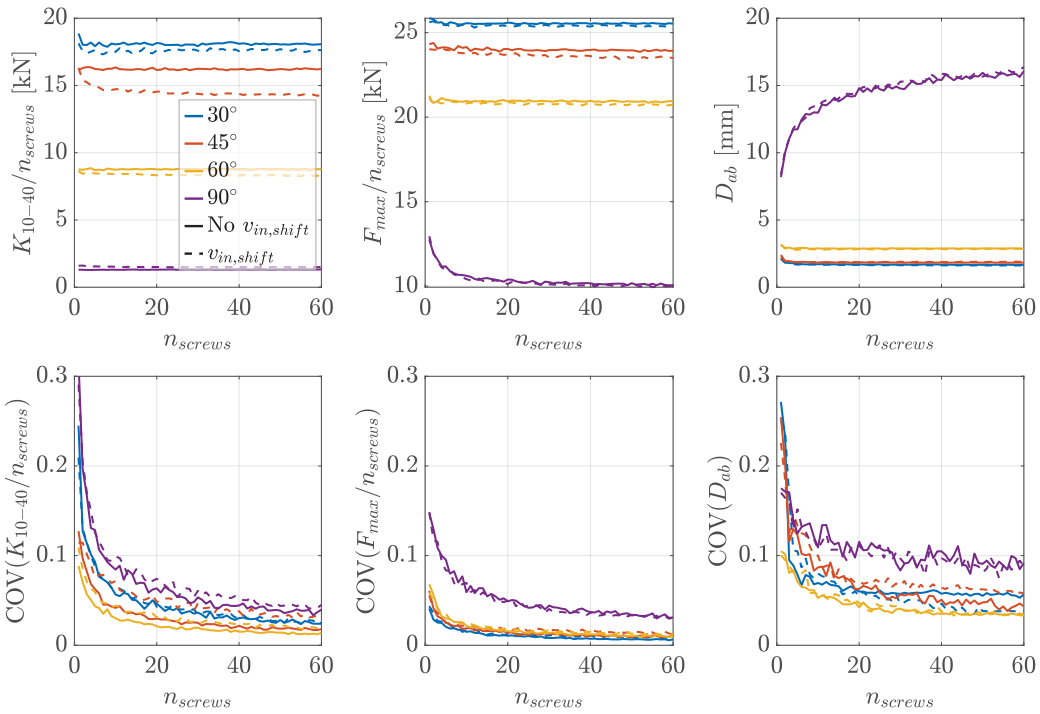


**Fig. 8.** Mean values scaled by number of screws $n_{screws}$ of elastic stiffness $K_{10-40}$, load-carrying capacity $F_{max}$ and mean values of absolute ductility $D_{ab}$ plotted against $n_{screws}$.
Solid lines refer to the case without the initial slip, dashed lines refer to the case with the initial slip.

or at 20% drop of the curve after the peak load. $v_y$ is calculated as the displacement at 50% of the load-carrying capacity [48]. Examples of curves and the associated variability of the scaled value of mean value of elastic stiffness $K_{10-40}/n_{screws}$, load-carrying capacity $F_{max}/n_{screws}$, and absolute ductility $D_{ab}$ for the case without and with the initial slip are reported in Fig. 8.

Increasing $n_{screws}$ has a small significant decrease on $K_{10-40}/n_{screws}$ for all the load-to-screw axis angles, while it does not affect $F_{\max}/n_{screws}$ and $D_{ab}$, for all the angles except 90°. For joints with load-to-screw axis angle of 90°, increasing the $n_{screws}$ noticeably reduces the mean values $F_{max}/n_{screws}$, and $D_{ab}$. Regarding variability, as $n_{screws}$ increases, the coefficient of variation (COV) for every angle falls with each additional screw. However, all of these effects diminish and eventually plateau: the mean values of $K_{10-40}/n_{screws}$, $F_{max}/n_{screws}$ and $D_{ab}$ converge, and COVs fall to minimal, asymptotic levels with increasing $n_{screws}$. This result can be expected, given the law of large numbers: as the number of screws grows, the overall response tends towards a Gaussian distribution whose standard deviation is inversely proportional to the square root of $n_{screws}$. Consequently, beyond a certain value of $n_{screws}$, diminishing changes in both mean values and COVs can be observed. Experiments and modelling conducted by Joyce [49,50] provide comparable evidence for groups of axially loaded screws and laterally loaded inclined screws: increasing the number of screws did not appreciably change the mean strength per screw, but it significantly reduced the characteristic (5% fractile) value of capacity, while the variability decreased. These outcomes are consistent with a parallel-system effect. The study also aligns with the findings of theoretical studies by Cao [51], who modelled group effects using the analogy with Daniel-system modelling.

The load–displacement behaviour for a representative set of 10 screws is shown in Fig. 9. These results are compared with the values of $K_{SLS}$ and the characteristic capacity $F_{Rk,multi}$ proposed by EC5. Both $K_{SLS}$ and $F_{Rk,multi}$ approximately match those obtained from the multi-screw model, except for the case of 60° and 90°, for which $K_{SLS}$ overestimates the mean stiffness of the joints. For steel-to-timber joints, EC5 recommends doubling the stiffness derived for timber-to-timber joints. For the joints with a load-to-screw axis of 90°, the stiffness is computed without the doubling factor in the subsequent analyses. This decision is justified by the fact that the empirical-probabilistic model of single-screw for this angle was calibrated on curves where the initial rigid region due to torque and friction was removed [36]. Another study observed that the EC5 doubling factor might, in some cases, overestimate the stiffness of steel-to-timber joints with screws [52].

### 3.3. Reliability of the structure

In this section, first, the results of a preliminary reliability (Section 3.3.1) and then the results of a full reliability analysis (Section 3.3.2) are reported. In the preliminary reliability analysis, the level of rigidity is set to a constant value ($\alpha = 0$) while the proportion of variable to total load is varied. Then the proportion of variable to total load is fixed ($Q_k/(Q_k + G_k)$ and the value of $\alpha$ is varied, assuming a linear behaviour of joints. The resulting $P_f$ curve serves as the reference for the subsequent full reliability analysis. In the full reliability analysis, the model is extended to include the joints nonlinear load–displacement behaviour together with their variability, providing a more realistic estimate of the reliability. Further parametric investigations quantify the influence of initial slip on $P_f$. The insights from the full reliability analysis are used to calibrate the ratio $K_{ULS}/K_{SLS}$.

#### 3.3.1. Preliminary reliability analysis

For a normal design situation, the target $P_f$ for a timber structure is $\approx 10^{-5}$ [44]. However, the actual value is dependent, amongst others, on the ratio between the permanent and the variable load: as the proportion of the variable load increases, $P_f$ increases. Typical ratios of variable to total load ($Q_k/(G_k + Q_k)$) for roof structure range between 0.5 and 0.9 [53].

In order to determine the reference $P_f$ for load ratios in that range, a study on a beam with a fixed level of rigidity ($\alpha = 0$, thus a simply supported beam) is conducted with $5 \cdot 10^{-7}$ runs of MCS. Across all the examined scenarios (load ratios between 0.1–0.9), $P_f$ of the beam remains bounded between $10^{-7}$ and $10^{-5}$ (Fig. 10(a)). For example,

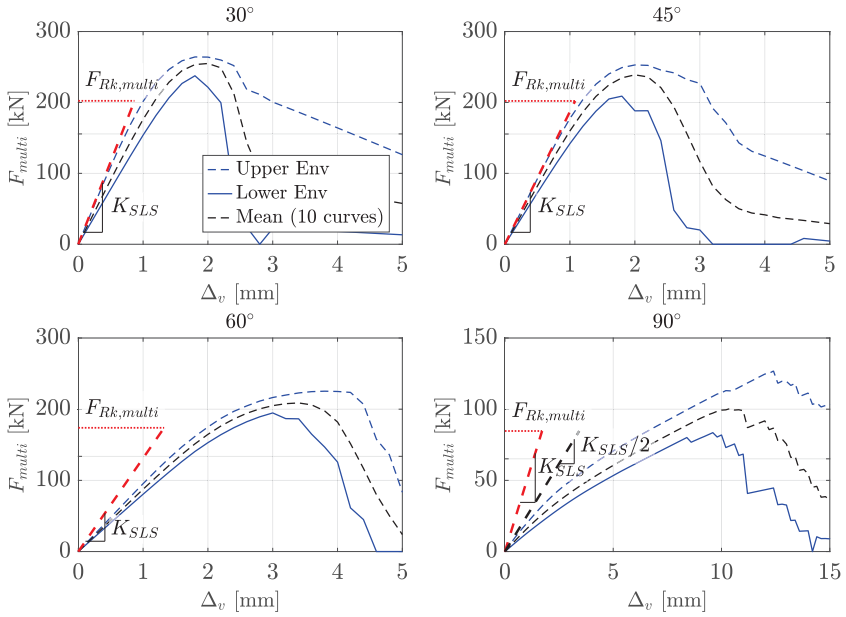


**Fig. 9.** Mean load–displacement curves with min–max envelopes for different load-to-screw axis angles ($n_{screws} = 10$) compared against the EC5 reference values $F_{Rk,multi}$ and $K_{SLS}$.

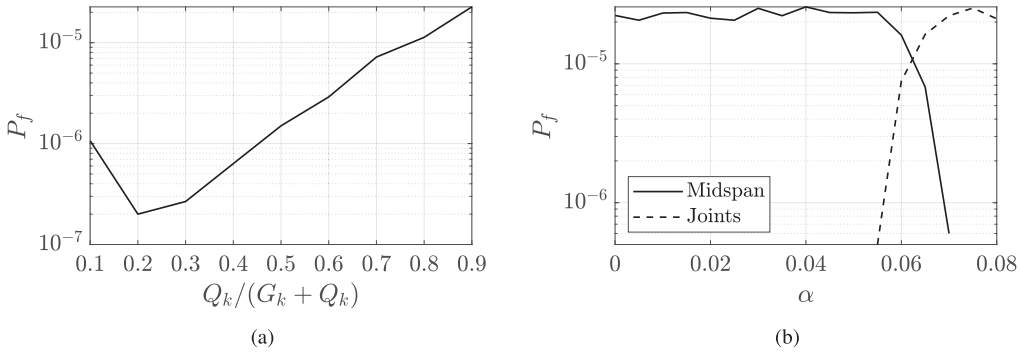


**Fig. 10.** (a) Baseline probability of failure vs. load ratio ($\alpha = 0$), (b) Baseline probability of failure vs. $\alpha$ ($Q_k/(G_k+Q_k) = 0.90$), failure location shifts from midspan to joints as $\alpha$ increases.

for a ratio of variable to total load equal to 0.10, $P_f = 2.2 \cdot 10^{-5}$. The higher $P_f$ observed in other studies (e.g. [53]) can be related to the additional consideration of model uncertainty, which is disregarded in this study for simplicity. The reference values of $P_f$ from this study are used as the target probability of failures for the calibration of the ratio $K_{ULS}/K_{SLS}$. $P_f$ of the system is studied, fixing $Q_k/(G_k + Q_k) = 0.90$ and varying $\alpha$. In this case, the joints are assumed linear-elastic, and the failure happens either at the midspan or at joints (in the beam). $P_f$ is invariant in relation to $\alpha$. The only variation is the location of failure: for $\alpha < 0.0633$ (moment at the joints equal to the moment at the midspan), the failure happens at midspan, for $\alpha > 0.0633$, the failure happens at the joints (Fig. 10(b)).

### 3.3.2. Full reliability analysis

In the full reliability analysis, the structural reliability of the system depicted in Fig. 3(a) is assessed using MCS with $2 \cdot 10^6$ runs. This sample size yields a precise estimate of the target probability of failure ($P_f = 2.2 \cdot 10^{-5}$), with a COV of ≈15%. This precision is acceptable for estimating rare events in structural reliability and was the criterion for selecting the sample size.

In the analytical model, once joints reach the ultimate rotation, the structure is idealised as a simply supported beam. For the design cases considered, exceeding the joints ultimate rotation always triggers failure of the structure: no moment redistribution occurs. Three distinct $P_f$ that correspond to three different failures are plotted: Midspan — bending failure at the beam midspan (label: midspan); Joints (beam) - failure at the joints in the beam (label: Joints (beam)); Joints — the ultimate rotation of joints is exceeded (label: Joints).

*Influence of the initial slip*

In a first step, a full reliability analysis across the range of $\alpha = (0.035 - 0.08)$ for the case of screws with load-to-screw axis angle of 90° is conducted to identify the possible influence of an initial slip in the joints. As can be seen in Fig. 11, incorporating an initial slip in the joints slightly increases $P_f$ for joints with lower values of $\alpha \leq 0.065$, while it decreases the probability of failure for higher values of $\alpha > 0.065$. Introducing a small value implies considering a lower stiffness at equilibrium, relaxing the end constraints and transferring moment towards midspan. This redistribution increases $P_f$ when ($\alpha \leq 0.065$), because midspan section is not detailed for the extra load, but reduces $P_f$ when the ($\alpha > 0.065$), since for these values midspan section has reserve capacity and the most loaded section shifts away from the joints.

Due to the limited value of the initial slip considered in the case of steel-to-timber joints with screws, no remarkable effect is observed on the probability of failure or failure mode of the structure. Therefore, the

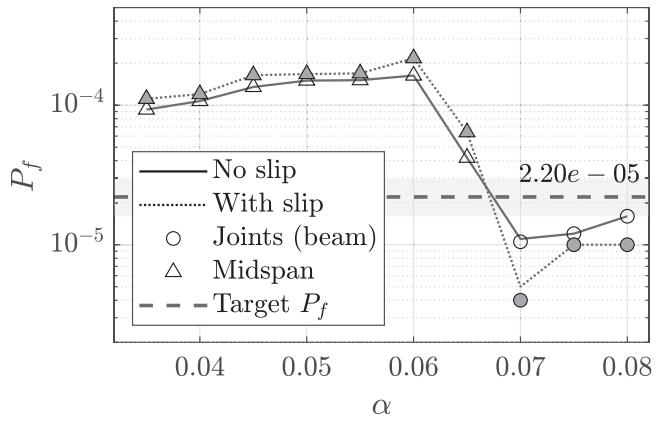


**Fig. 11.** Effect of initial slip on the probability of failure of the structure versus $\alpha$ ($K_{ULS}/K_{SLS} = 1$). Marker shapes indicate the failure location: at joints in the beam (circle) or midspan (triangle).

initial slip is not taken into account in the further steps of the analysis. It is worth noting that workmanship may induce larger slips, and alternative distributions (e.g., Beta or symmetric Gaussian/triangular) could be employed. When the resulting distribution entails a higher mean slip or, for a fixed mean, places more probability on larger slips, the associated stiffness reduction is greater and the trend in $P_f$ might be accentuated, thereby increasing $P_f$ for $\alpha \leq 0.065$ and decreasing $P_f$ for $\alpha > 0.065$. Conversely, distributions concentrating probability on smaller slips would attenuate this effect.

*Influence of the ratio $K_{ULS}/K_{SLS}$*

The impact of the ratio $K_{ULS}/K_{SLS}$ on the reliability of the structure is studied by comparing two cases: the code-prescribed ratio of 2/3 and the theoretical upper-bound ratio of 1 for the feasible values of $\alpha$. The results are illustrated in Fig. 12.

For the case $K_{ULS}/K_{SLS} = 2/3$, $P_f$ is above the target probability value ($P_f = 2.20 \cdot 10^{-5}$) for $\alpha < 0.065$. In particular, $P_f$ increases by a factor of ≈2-2.2 (being approximately in the range between $4 \cdot 10^{-5}$ and $4.90 \cdot 10^{-5}$). Then, with increasing values of $\alpha$, $P_f$ converges towards the target value (Fig. 12(a)). For the case $K_{ULS}/K_{SLS} = 1$, not accounting for any reduction in stiffness at ULS increases $P_f$ compared to the case $K_{ULS}/K_{SLS} = 2/3$ for $\alpha$ between 0.035 and 0.065. For $\alpha \geq 0.07$, the reduction is unnecessary. $P_f$ is unchanged, or even increases, like for the case of 60° and 90° (Fig. 12(b)). This results in an uneconomical design of joints since it would require more screws without a benefit in terms of reliability.

The reduction in $P_f$ for joints of higher rigidity, passing from hinged to clamped joints, is due to the fact that the failure moves from midspan to the joints in the beam. This is illustrated in Fig. 13, where equilibrium points at failure are shown for three different values of $\alpha$ (0.02, 0.06, 0.075). For representational purposes, the lowest $\alpha = 0.02$ value is used, even though the design would typically be governed by the SLS. The green dots indicate equilibrium points associated with failure at midspan ($M_{E,field}$), while the blue dots represent equilibrium points that cause failure at the joints in the beam ($M_{E,joints}$). Finally, the green dots also show the corresponding values of the equilibrium points in the joints when failure occurs at midspan. When $\alpha < 0.065$, the equilibrium at ULS falls within the post-elastic range (Fig. 13(a) and Fig. 13(b)) of the joints curve. Therefore, $P_f$ is sensitive to the 2/3 ratio, yet even then, it never quite meets the target $P_f$. Increasing $\alpha$ means that the equilibrium under ULS loading moves more and more into the elastic range (Fig. 13(c)). Hence, the $K_{ULS}/K_{SLS} = 2/3$ stiffness ratio is both redundant for joints with $\alpha \geq 0.07$ close to the clamped condition and potentially unsafe for semi-rigid ones. $P_f$ remains constant for very stiff joints (i.e., as more screws are added) because the moments at joints and midspan become progressively less sensitive to changes in joint stiffness (see Fig. 3(b)) the equilibrium points fall inside the elastic region of joints. The results confirm the importance and the influence of the nonlinear behaviour for semi-rigid joints on the reliability of timber structures already observed in previous studies [8,30]. However, in these studies, a larger effect (≈3.7 increase from the target $P_f$) was observed. In contrast, the stiffness-based modelling strategy employed herein yields a remarkable yet smaller change (≈2.2 increase from the target $P_f$ for the worst-case scenario). This reduction in effect may be due to the different structural systems and types of joints studied, as well as to different assumptions about joint behaviour (pinned/clamped assumptions in design, use of elastic-perfectly plastic behaviour).

### 3.4. Calibration of $K_{ULS}/K_{SLS}$

The ratio $K_{ULS}/K_{SLS}$ is calibrated in order to meet the target reliability by means of a bisection and grid algorithm. The algorithm is configured to run for a maximum of 5 iterations and was terminated once the computed failure probability came within a specified threshold of the target value. The ratio $K_{ULS}/K_{SLS}$ can be expressed in several equivalent ways:

1. As a function of the relative joint stiffness (Fig. 14(a)–Fig. 14(b)). The relative joint stiffness can be expressed in terms of $\alpha$ or $k_b$.
2. As a function of the utilisation ratio $M_{Ed,joints}/M_{Rd,joints}$ (Fig. 14(c)), as it is currently adopted by EC3 for moment-resisting steel joints [21].
3. As a function of dimensionless required joint rotation $\theta_{req,d}/\theta_{max,d}$ (Fig. 14(d)). $\theta_{req,d}$ is the design value of the required rotation at joints, and $\theta_{max,d}$ is the design value of the rotation at joints of the corresponding simply supported beam.

The ratio $K_{ULS}/K_{SLS}$ increases with increasing $\alpha$ (or, equivalently, the dimensionless stiffness ratio $k_b$), with decreasing $M_{Ed,joints}/M_{Rd,joints}$ and with decreasing $\theta_{req,d}/\theta_{max,d}$. Outside the narrow interval $0.063 < \alpha < 0.067$ the curve is almost flat, yielding similar values for the extremes of the examined $\alpha$ range. Within that range, however, the ratio increases sharply: even a slight change in $\alpha$ produces a large change in $K_{ULS}/K_{SLS}$. For $\alpha \leq 0.063$, $K_{ULS}/K_{SLS}$ assumes an average value of 0.56, while for $\alpha \geq 0.067$, $K_{ULS}/K_{SLS}$ is always 1.

## 4. Conclusions

The nonlinear behaviour of joints significantly influences the reliability of statically indeterminate timber structures. EC5 takes into account the nonlinear behaviour of joints, assuming a reduced value of the stiffness of joints at the ultimate limit state, as two-thirds of the value at the serviceability limit state. Modern designs often use inclined self-tapping screw joints for their high stiffness and capacity. This study first models the load–displacement response of multi-screw joints, then derives the moment–rotation curve via the component method. The curve is subsequently employed in a Monte Carlo reliability analysis of a statically indeterminate timber beam under a uniformly distributed load. The conclusions regarding the outcomes of the reliability of the statically indeterminate beam and the consequent calibration of the ratio $K_{ULS}/K_{SLS}$ are the following:

1. The adequate ratio $K_{ULS}/K_{SLS}$ heavily depends on the type and nonlinear behaviour of the joints. A unique value cannot cover all the joint typologies.
2. Setting the ratio $K_{ULS}/K_{SLS} = 2/3$ results in an underestimate of the probability of failure for joints with load-to-screw axis of 90° when $\alpha < 0.07$, resulting in unsafe designs, and it is redundant when $\alpha \geq 0.07$, since the probability remains constant or either increases compared to the case when $K_{ULS}/K_{SLS} = 1$, but the joints require more screws.

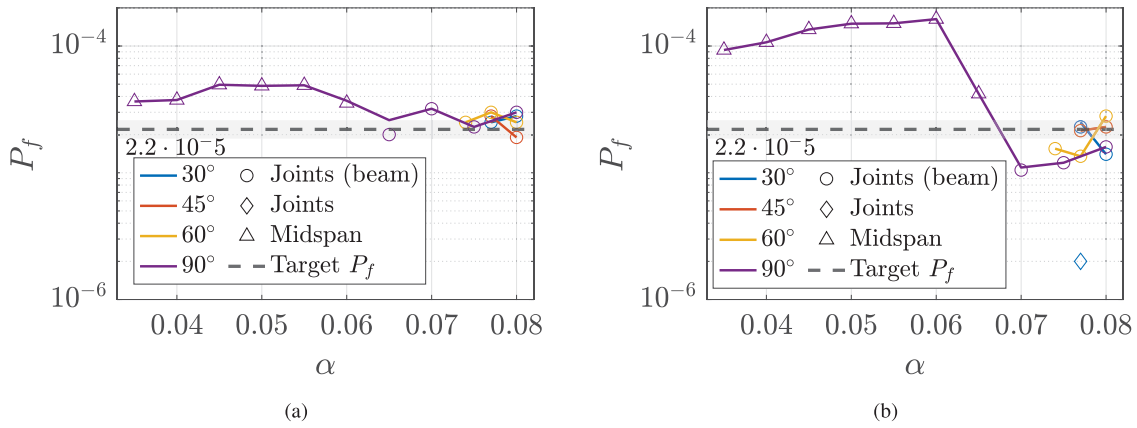


**Fig. 12.** Probability of failure versus $\alpha$. (a) $K_{ULS}/K_{SLS} = 2/3$, (b) $K_{ULS}/K_{SLS} = 1$. Marker shapes indicate the failure location: at joints in the beam (circle), midspan (triangle), due to the exceedance of the ultimate rotation of joints (diamond).

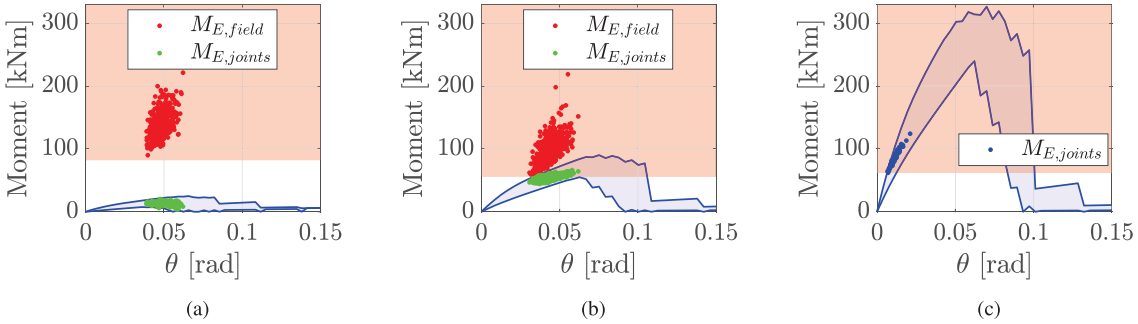


**Fig. 13.** Moment–rotation diagram and equilibrium points for the angle 90°. To make the failure points visible, the reliability analysis was conducted assuming larger loads. (a) $\alpha = 0.02$, (b) $\alpha = 0.06$, (c) $\alpha = 0.075$. Blue dots: failure at joints in the beam; Red dots: failure at midspan; Green dots: equilibrium points at the joints when failure is at midspan.

3. Depending on the chosen value of $\alpha$, the coefficient can assume different values:
   - For $\alpha > 0.077$ (load-to-screw axis 30° and 45°), $\alpha > 0.074$ (load-to-screw axis 60°, and $\alpha > 0.067$ (load-to-screw axis 90°), the joint remains in its linear-elastic range, thus $K_{ULS}/K_{SLS} = 1$.
   - For joints with load-to-screw axis angle of 90°, for $\alpha \leq 0.063$, the calibrated ratio $K_{ULS}/K_{SLS}$ assumes an average value of 0.56.
   - For joints with load-to-screw axis angle of 90°, for $\alpha = 0.063 - 0.067$ the ratio $K_{ULS}/K_{SLS}$ is very sensitive to $\alpha$. In this range, calibration shows that the optimal ratio falls between 0.56 and 1.00.

## 5. Limitations and future work

This study constitutes a transferable probabilistic framework that could be extended to other joint types and structures. The probabilistic model of the structure is benchmarked against the recognised value of target probability of failure (JCSS [44]), showing consistency with $P_f \approx 10^{-5}$ for ULS. However, it is still characterised by some limitations due to (i) a limited number of experiments on which the single-screw model is based, (ii) additional possible failure modes, (iii) not accounted interactions among screws due to spacing. In fact, the single-screw joint model is developed based on a limited number of experiments. Additional tests are needed to confirm the validity of the model. As a consequence of the limited number of experiments and lack of data, the correlations between model parameters and timber properties are uncertain. Other failure modes (e.g., shear, brittle failures) and their effect on reliability were not studied. Results apply to joints with larger-than-code spacings; closer spacing increases screw interaction, alters joint behaviour, and raises the risk of brittle failures, which can reduce beam reliability. Therefore, future research should aim to fill these gaps and reduce the uncertainties in the structural probabilistic model.

## CRediT authorship contribution statement

**Dorotea Caprio:** Writing – review & editing, Writing – original draft, Visualization, Validation, Software, Resources, Methodology, Investigation, Formal analysis, Data curation, Conceptualization. **Robert Jockwer:** Writing – review & editing, Supervision, Project administration, Methodology, Funding acquisition, Conceptualization.

## Declaration of Generative AI and AI-assisted technologies in the writing process

The authors used ChatGPT to occasionally refine grammar and readability. After using this tool, the authors reviewed and edited the content as needed and take full responsibility for the content.

## Declaration of competing interest

The authors declare that they have no known competing financial interests or personal relationships that could have appeared to influence the work reported in this paper.

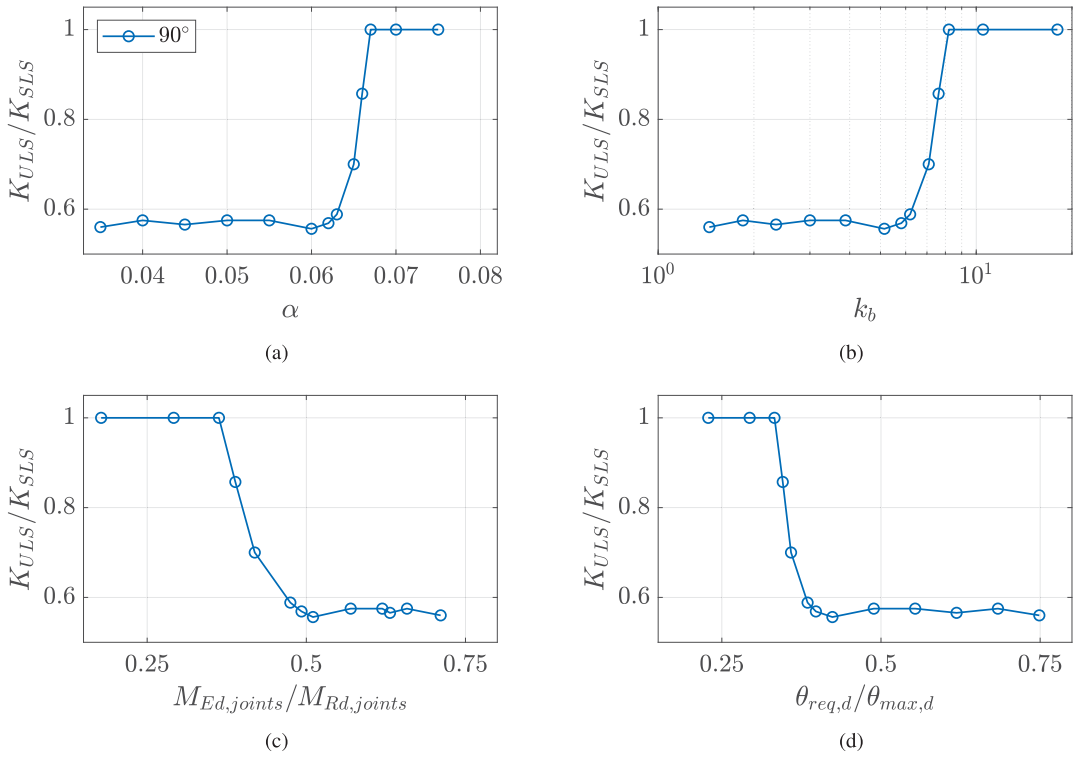


**Fig. 14.** Calibrated values of ratio $K_{ULS}/K_{SLS}$ as function of: (a) rigidity level $\alpha$, (b) relative stiffness $k_b$, (c) utilisation moment ratio, $M_{Ed,joints}/M_{Rd,joints}$, (d) rotation ratio $\theta_{req,d}/\theta_{max,d}$.

## Acknowledgements

This research was funded by the FORMAS project "RelyConnect" (2023-01603), Svensk Trä, the Swedish association of the timber industries, and TMF, the Swedish Federation of Wood and Furniture Industry (Trä och Möbelföretagen). Computations were run on NAISS, the National Academic Infrastructure for Supercomputing in Sweden.

## Data availability

Data will be made available on request.

## References

[1] Gotz K-H, Hoor D, Mohler K, Natterer J. Timber design and construction sourcebook: A comprehensive guide to methods and practice. McGraw-Hill; 1989.

[2] Lawrence A. Recommendations for the design of complex indeterminate timber structures. In: Materials and joints in timber structures. Springer Netherlands; 2014, p. 129–34. http://dx.doi.org/10.1007/978-94-007-7811-5_12.

[3] Larsen H, Jensen J. Influence of semi-rigidity of joints on the behaviour of timber structures. Prog Struct Eng Mater 2000;2:267–77.

[4] EN 1995-1-1: Eurocode 5: Design of timber structures - Part 1-1: General and rules for buildings. Brussels, Belgium: European Committee for Standardization CEN; 1995, EN 1995-1-1.

[5] Ehlbeck J, Werner H. Untersuchungen über die Tragfähigkeit von Stabdübelverbindungen. Holz Als Roh- Und Werkst 1988;46(8):281–8. http://dx.doi.org/10.1007/BF02615055.

[6] Mack JJ. The strength and stiffness of nailed joints under short-duration loading. Division of forest products technological paper, Melbourne, Australia: Commonwealth Scientific and Industrial Research Organization; 1966.

[7] Hendawi S, Frangopol DM. System reliability and redundancy in structural design and evaluation. Struct Saf 1994;16(1):47–71. http://dx.doi.org/10.1016/0167-4730(94)00027-N.

[8] Caprio D, Jockwer R, Al-Emrani M. Reliability of statically indeterminate timber structures: Modelling approaches and sensitivity study. In: Current perspectives and new directions in mechanics, modelling and design of structural systems: proceedings of the 8th international conference on structural engineering, mechanics and computation. CRC Press; 2022, p. 1649–55. http://dx.doi.org/10.1201/9781003348443-270.

[9] Acler E. Nanyang Technological University Sports Hall – Singapore. In: Proceedings of the 23rd internationales Holzbau-forum IHF. Garmisch-Partenkirchen, Germany; 2017.

[10] Rebhahn J, Stenberg Ringnér M. World of Volvo, Gothenburg - pushing the boundaries. In: Proceedings of the 26th internationales holzbau-forum IHF. Innsbruck, Austria; 2022.

[11] Cramer CO. Load distribution in multiple-bolt tension joints. J Struct Div 1968;94(5):1101–17. http://dx.doi.org/10.1061/JSDEAG.0001946.

[12] Wilkinson TL. Load distribution among bolts parallel to load. J Struct Eng 1986;112(4):835–52. http://dx.doi.org/10.1061/(ASCE)0733-9445(1986)112:4(835).

[13] Zahn JJ. Design equation for multiple-fastener wood connections. J Struct Eng 1991;117(11):3477–86. http://dx.doi.org/10.1061/(ASCE)0733-9445(1991)117:11(3477).

[14] Jorissen A. Double-shear timber connections with dowel-type fasteners [Ph.D. thesis], Delft, The Netherlands: Delft University of Technology; 1998.

[15] Soltis LA, Wilkinson TL. Bolted-connection design. Tech. Rep. FPL-GTR-54, Madison, WI: U.S. Department of Agriculture, Forest Service, Forest Products Laboratory; 1987, http://dx.doi.org/10.2737/FPL-GTR-54.

[16] Bader T, Bocquet J-F, Schweigler M, Lemaitre R. Numerical modeling of the load distribution in multiple fastener connections. 2018, p. 221–39.

[17] Schweigler M, Bader TK, Hochreiner G. Engineering modeling of semi-rigid joints with dowel-type fasteners for nonlinear analysis of timber structures. Eng Struct 2018;171:123–39. http://dx.doi.org/10.1016/j.engstruct.2018.05.063.

[18] Lauritzen Jensen J. Dowel-type fastener connections in timber structures subjected to short-term loading: Ph.D. thesis [Ph.D. thesis], (237). Denmark: SBI forlag; 1994.

[19] Niemz P, Teischinger A, Sandberg D, editors. Springer handbook of wood science and technology, In: Springer handbooks, 1st ed. Cham: Springer; 2023, http://dx.doi.org/10.1007/978-3-030-81315-4.

[20] Rebouças AS, Mehdipour Z, Branco JM, Lourenço PB. Ductile moment-resisting timber connections: A review. Buildings 2022;12(22). http://dx.doi.org/10.3390/buildings12020240.

[21] EN 1993-1-1: Eurocode 3: Design of steel structures - Part 1-1: General rules and rules for buildings. Brussels, Belgium: European Committee for Sandardization CEN; 2004.

[22] Xu BH, Bouchaïr A, Racher P. Analytical study and finite element modelling of timber connections with glued-in rods in bending. Constr Build Mater 2012;34:337–45. http://dx.doi.org/10.1016/j.conbuildmat.2012.02.087.
[23] Yang H, Liu W, Ren X. A component method for moment-resistant glulam beam–column connections with glued-in steel rods. Eng Struct 2016;115:42–54. http://dx.doi.org/10.1016/j.engstruct.2016.02.024.
[24] Stamatopoulos H, Hegeir OA, Malo KA. Analysis and design aspects of moment-resisting beam-to-column timber connections with inclined threaded rods: from fastener level to construction level. In: World conference on timber engineering. Oslo, Norway; 2023, p. 1206–15. http://dx.doi.org/10.52202/069179-0165.
[25] Rebouças AS, Branco JM, Simões R, Lourenço PB, Diógenes HJF. Design of stiffened end-plate moment-resisting steel-timber joints with multiple bonded-in rods using the component method. Eng Struct 2025;341:120793. http://dx.doi.org/10.1016/j.engstruct.2025.120793.
[26] Krug S, Jaaranen J, Fink G, Schänzlin J. Determination of the moment–rotation relation of continuous timber–concrete composite floors based on the component method. Structures 2024;69:107365. http://dx.doi.org/10.1016/j.istruc.2024.107365.
[27] Hansson M, Ellegaard P. System reliability of timber trusses based on non-linear structural modelling. Mater Struct 2006;39(6):593–600. http://dx.doi.org/10.1617/s11527-006-9098-8.
[28] Kirkegaard PH, Sørensen JD, Čizmar D, Rajčić V. System reliability of timber structures with ductile behaviour. Eng Struct 2011;33(11):3093–8. http://dx.doi.org/10.1016/j.engstruct.2011.03.011.
[29] Brühl F, Kuhlmann U, Jorissen A. Consideration of plasticity within the design of timber structures due to connection ductility. Eng Struct 2011;33:3007–17. http://dx.doi.org/10.1016/j.engstruct.2011.08.013.
[30] Schilling S. Structural behaviour and reliability of timber trusses with dowelled steel-to-timber connections [Ph.D. thesis], ETH Zurich; 2022, http://dx.doi.org/10.3929/ethz-b-000538109.
[31] Flatscher G. Evaluation and approximation of timber connection properties for displacement-based analysis of CLT wall systems. In: Monographic series TU graz: timber engineering & technology, vol. 6, Verlag der Technischen Universität Graz; 2017.
[32] Klasson A, Crocetti R, Björnsson I, Frühwald Hansson E. Design for lateral stability of slender timber beams considering slip in the lateral bracing system. Structures 2018;16:157–63. http://dx.doi.org/10.1016/j.istruc.2018.09.007.
[33] Jorissen A, Fragiacomo M. General notes on ductility in timber structures. Engineering Structures 2011;33:2987–97. http://dx.doi.org/10.1016/j.engstruct.2011.07.024.
[34] Šabatka L, Kolaja D, Vild M, Wald F, Kuříková M, Kabeláč J. Influence of joint stiffness on design of steel members. In: Advances and trends in engineering sciences and technologies III: proceedings of the 3rd international conference on engineering sciences and technologies. CRC Press; 2019, p. 247–52. http://dx.doi.org/10.1201/9780429021596-39.
[35] Caprio D, Jockwer R, Ringhofer A. Parametrization of the non-linear behaviour of timber joints with self-tapping screws. In: Proceedings of meeting no. 57th of the international network on timber engineering research (INTER), paper no. 57-7-7. Padua, Italy; 2024.
[36] Caprio D, Jockwer R. Experimental investigation and probabilistic modelling of the load–displacement behaviour of steel-to-timber joints with self-tapping screws. Constr Build Mater 2025;489:141970. http://dx.doi.org/10.1016/j.conbuildmat.2025.141970.
[37] EN 12512: Timber structures - Test methods - cyclic testing of joints made with mechanical fasteners. Bruxelles, Belgium: European Committee for Standardization CEN; 2002.
[38] Richard RM, Abbott BJ. Versatile elastic–plastic stress–strain formula. J Eng Mech Div 1975;101(4):511–5. http://dx.doi.org/10.1061/JMCEA3.0002047.
[39] Song J, Kang W-H, Lee Y-J, Chun J. Structural system reliability: Overview of theories and applications to optimization. ASCE-ASME J Risk Uncertain Eng Syst Part A: Civ Eng 2021;7(2):01122. http://dx.doi.org/10.1061/AJRUA6.0001122.
[40] Fauriat W, Gayton N. AK-SYS: An adaptation of the AK-MCS method for system reliability. Reliab Eng Syst Saf 2014;123:137–44. http://dx.doi.org/10.1016/j.ress.2013.10.010.
[41] Benjamin JR, Cornell CA. Probability, statistics, and decision for civil engineers. 1st ed.. Burlington, MA: Courier Corporation; 2014.
[42] Batho C, Rowan HC. The analysis of the moments in the members of a frame having rigid or semi-rigid connections, under vertical loads. Second report, London, England: Steel Structures Research Committee; 1934.
[43] Leijten AJM. Requirements for moment connections in statically indeterminate timber structures. Eng Struct 2011;33(11):3027–32. http://dx.doi.org/10.1016/j.engstruct.2011.03.014.
[44] Probabilistic model code. Tech. rep., Joint Committee on Structural Safety (JCSS); 2006.
[45] Ross SM. A first course in probability. 5th ed.. Upper Saddle River, NJ: Prentice Hall; 1998.
[46] EN 1990:2002: Basis of structural design. Brussels, Belgium: European Committee for Standardization CEN; 2002.
[47] Jockwer R, Caprio D, Jorissen A. Evaluation of parameters influencing the load–deformation behaviour of connections with laterally loaded dowel-type fasteners. Wood Mater Sci Eng 2021;1–14. http://dx.doi.org/10.1080/17480272.2021.1955297.
[48] Karacabeyli E, Ceccotti A. Quasi-static reversed-cyclic testing of nailed joints. In: Proceedings of the CIB-W18 meeting 29/29-7-7. Bordeaux, France; 1996.
[49] Joyce T, Chui YH. Group effects in axially loaded self-tapping screw connections. Eng Struct 2022;251:113537. http://dx.doi.org/10.1016/j.engstruct.2021.113537.
[50] Joyce T, Chui Y. A systems approach to evaluating group effect factors with simulated inclined self-tapping screw connections. Can J Civ Eng 2025;52:1292–304. http://dx.doi.org/10.1139/cjce-2024-0354.
[51] Cao AS, Thöns S, Jockwer R, Palma P. System effects in timber connections comprising multiple fasteners. In: Proceedings of the 14th international conference on structural safety and reliability. Los Angeles, CA, USA: ASCE; 2025, p. 1–12. http://dx.doi.org/10.23967/icossar.2025.096.
[52] Wang C-L, Lyu J, Zhao J, Yang H. Experimental investigation of the shear characteristics of steel-to-timber composite joints with inclined self-tapping screws. Eng Struct 2020;215:110683. http://dx.doi.org/10.1016/j.engstruct.2020.110683.
[53] Jockwer R, Fink G, Köhler J. Review of the reliability of timber structures in the 2020s. In: Proceedings of meeting no. 53rd of the international network on timber engineering research. 2020, p. 29–45.